

Analyst

Accepted Manuscript



This is an *Accepted Manuscript*, which has been through the Royal Society of Chemistry peer review process and has been accepted for publication.

Accepted Manuscripts are published online shortly after acceptance, before technical editing, formatting and proof reading. Using this free service, authors can make their results available to the community, in citable form, before we publish the edited article. We will replace this *Accepted Manuscript* with the edited and formatted *Advance Article* as soon as it is available.

You can find more information about *Accepted Manuscripts* in the [Information for Authors](#).

Please note that technical editing may introduce minor changes to the text and/or graphics, which may alter content. The journal's standard [Terms & Conditions](#) and the [Ethical guidelines](#) still apply. In no event shall the Royal Society of Chemistry be held responsible for any errors or omissions in this *Accepted Manuscript* or any consequences arising from the use of any information it contains.

Applications of Tunable Resistive Pulse Sensing

Eva Weatherall^{1,2} and Geoff R. Willmott^{1,3,†}

¹The MacDiarmid Institute for Advanced Materials and Nanotechnology, School of Chemical and Physical Sciences, Victoria University of Wellington

²Callaghan Innovation, PO Box 31-310, Lower Hutt 5040, New Zealand

³The Departments of Physics and Chemistry, The University of Auckland, New Zealand

[†] Corresponding author

Email: g.willmott@auckland.ac.nz

Phone: (64) (0)9 9737599

Fax: (64) (0)9 3737445

Tunable resistive pulse sensing (TRPS) is an experimental technique that has been used to study and characterise colloidal particles ranging from approximately 50 nm in diameter up to the size of cells. The primary aim of this Review is to provide a guide to the characteristics and roles of TRPS in recent applied research. Relevant studies reflect both the maturation of the technique and the growing importance of submicron colloids in fields such as nanomedicine and biotechnology. TRPS analysis of extracellular vesicles is expanding particularly swiftly, while TRPS studies also extend to on-bead assays using DNA and aptamers, drug delivery particles, viruses and bacteria, food and beverages, and superparamagnetic beads. General protocols for TRPS measurement of particle size, concentration and charge have been developed, and a summary of TRPS technology and associated analysis techniques is included in this Review.

Introduction

Tunable resistive pulse sensing (TRPS) is an experimental technique capable of particle-by-particle detection and analysis of submicron colloids and bioparticles.¹⁻¹³ The purpose of this Review is to provide the practising researcher with a guide to the characteristics of TRPS, with emphasis on the roles it has played in recent applied research. The Review covers TRPS research into a wide range of particle types, encompassing numerous research fields and research objectives. It draws on information sources that will be of specific relevance to particular TRPS investigations, and also those that promote interdisciplinary understanding of the technique. The Review demonstrates the challenges of colloidal characterization, such as the often complex nature of raw samples (*e.g.* bodily fluids), the importance of understanding the distinct principles behind different measurement techniques, and the sheer variety of interesting particle types.

TRPS is a variant of resistive pulse sensing (RPS), a family of analytic techniques in which particles are suspended in aqueous electrolyte and pass through a single pore in a membrane. An electric potential applied across the membrane drives an ionic current which is disrupted when a particle passes through the pore, generating a resistive pulse (Figure 1(a)). RPS has enabled high throughput particle-by-particle sensing and analysis of cells since the 1950s,¹⁴ submicron particles including viruses since the 1970s,^{15,16} and particles as small as single molecules over the past decade or so, with particularly intense interest in possible nanopore-based DNA sequencing. Recent reviews have covered analysis of nucleic acids using biological nanopores¹⁷ and the broader field of molecular-scale RPS.^{18,19,20}

TRPS¹⁻¹³ is distinctive because the membrane is an elastomer.¹¹ When the membrane is stretched on macroscopic length scales, the nanoscale dimensions of the sensing pore are mechanically 'tuned'.^{12,}
¹³ The most immediate advantages of tuning are pragmatic, such as recovery from a blockage when the membrane is stretched. Also, the signal-to-noise ratio of the resistive pulse signal can be

1
2
3 optimised *in situ*, during an experiment. TRPS therefore has a flexibility unavailable with static pores
4
5 used for RPS.
6
7

8
9 First reported almost a decade ago,¹ TRPS reached essentially its present form by 2010² and there
10 are now established TRPS protocols for measurement of particle size,³ concentration^{2, 4, 5} and
11 charge.⁶⁻⁸ Much of this development work has used spherical polystyrene (PS) colloids, commercially
12 available as size standards. The range of particle sizes measured using TRPS spans from micrometers
13 down to ~50 nm, covering approximately two orders of magnitude in length scale and bridging the
14 gap between single molecules and cells.⁹ A variety of electrolytes can be used, including those which
15 replicate physiological conditions, and 100 mM salt is typical. The accessible range of particle
16 concentrations is approximately $10^5 - 10^{12}$ mL⁻¹.²¹ TRPS has sometimes been called scanning ion
17 occlusion spectroscopy (SIOS), and tunable pores have also been known as resizable (nano)pores.
18
19

20
21 This Review does not detail RPS work at comparable length scales using (static) solid-state pores.
22

23 Such studies have made use of pore materials including silicon-based membranes,^{22, 23} carbon
24 nanotubes,^{24, 25} and lithographically moulded²⁶ and track-etched^{20, 27, 28} polymers. Glass pores have
25 been made by laser machining,²⁹⁻³¹ the pipette pulling technique,^{32, 33} and moulding around a sharp
26 wire tip.^{34, 35, 36} Henriquez *et al.*³⁷ and more recently Luo *et al.*³⁸ have reviewed aspects of static RPS
27 experiments. TRPS has a particular similarity to RPS studies in which the pore geometry is conical.^{20,}
28
29

30
31
32
33
34
35
36
37
38
39
40
41
42
43
44 27, 30, 32, 36, 39, 40
45
46
47

48 The first section of this Review (“Technical aspects”) introduces the technology by briefly recounting
49 descriptions of TRPS and basic sensing characteristics, and then identifying areas of ongoing
50 technical development. Comparisons with other methods are reviewed, revealing some advantages
51 and distinct characteristics of TRPS. The second section (“Applications”) reviews application of TRPS
52 to a broad range of particle types. This section summarizes important results and serves as a guide
53
54
55
56
57
58
59
60

both to those studies most relevant to each specific experimental area, and to perspectives which may apply across different fields of research. Studies are broadly classified by application area: diagnostics and genomics, extracellular vesicles, nanomedicine, phages, viruses and bacteria, and others. Inevitably, the boundaries between classifications can be indistinct, as in the case of structurally-similar EVs, liposomes and emulsions.

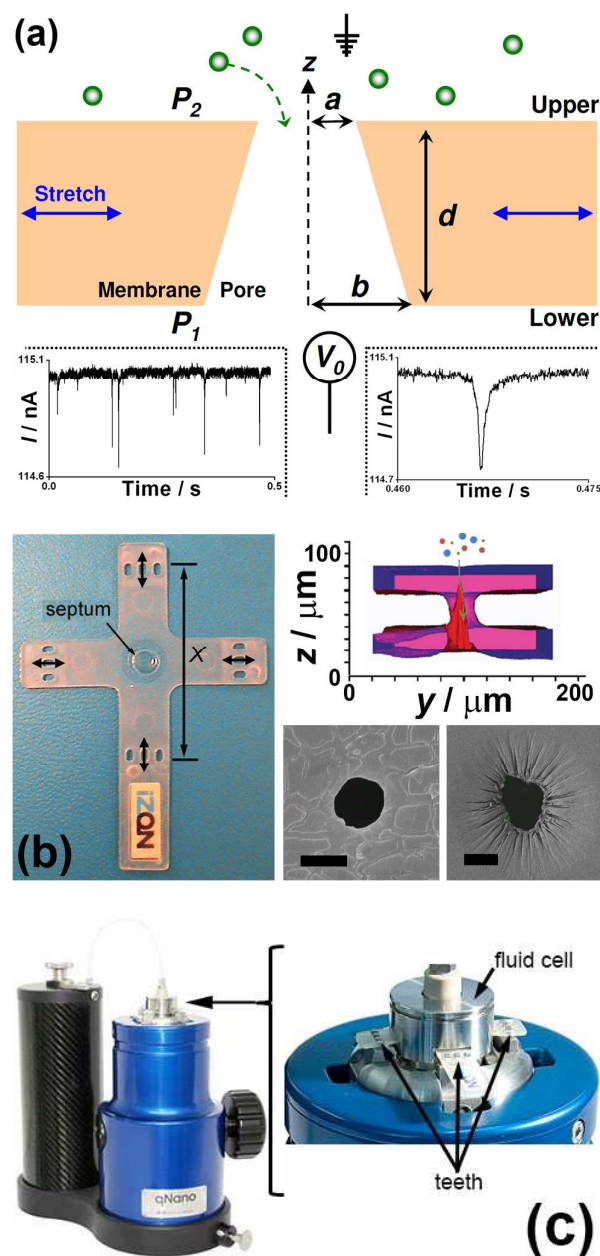


Figure 1: TRPS, tunable pore specimens, and typical apparatus. (a) Schematic section through a tunable pore, indicating experimental variables usually used in TRPS analysis. The conical pore of

1
2
3 length d has openings of radius a and b , and is assumed to be symmetric about the cylindrical z -axis.
4
5 Potential V_0 and pressure $P_2 - P_1$ are applied across the membrane. Lower left, typical experimental
6
7 data showing resistive pulses. Lower right, one pulse in greater detail. Adapted from Somerville *et*
8
9 *al.*⁴¹ (b) Specimen imaging. Left, a thermoplastic polyurethane specimen. X is ~ 42 mm for an
10
11 unstretched specimen, and the pore is located near the centre of the ~ 200 μm thick circular septum.
12
13 Reproduced from Willmott *et al.*¹³ Right upper, reconstruction of a pore cross-section from confocal
14
15 microscopy, adapted from Kozak *et al.*⁹ Right lower, SEM images of smaller (left) and larger (right)
16
17 openings of a pore stretched to $X = 45$ mm (scale bars 1 μm and 20 μm respectively), adapted from
18
19 Willmott *et al.*¹³ (c) The *qNano* (left, Izon Science) TRPS apparatus, and (right) the magnified fluid
20
21 cell. Ag/AgCl electrodes contact each half of the cell. Actuation is achieved by turning the handle on
22
23 the side of the *qNano*, which moves teeth placed in the specimen. The black cylindrical VPM
24
25 connects to the top of the fluid cell via tubing. Adapted from Willmott *et al.*¹³ and Weatherall *et al.*⁸
26
27
28
29
30

31 Technical aspects

32 Specimens, apparatus and stretching

33
34
35 Tunable pore specimens are formed by controlled puncture of a thermoplastic polyurethane (TPU)
36
37 membrane using a chemically etched tungsten needle.¹ This process is relatively efficient in
38
39 comparison with the intensive techniques necessary to make pores for detecting single molecules¹⁸
40
41 – such as electron or ion beam lithography, or use of biological pores. An approximately conical hole
42
43 is produced, with larger and smaller pore openings (Figures 1(a) and 1(b)). Depending on the needle⁸
44
45 and fabrication parameters, commercially-available pores are given a rating indicating their relative
46
47 size, and therefore the particle size they are most suited to sensing. Scanning electron microscopy
48
49 (SEM)^{2, 3, 7, 11, 12, 41-43} has enabled imaging of a variety of pores at different stretches, and
50
51 measurement of pore opening sizes, while confocal microscopy can provide three-dimensional
52
53 information^{2, 9, 44} and atomic force microscopy (AFM) has also been used for imaging (Figure 1(b)).¹²
54
55
56
57
58
59
60

1
2
3
4
5 The membrane is the ~ 200 μm thick central septum of an injection-moulded sample (Figure 1(b)).
6
7 Each cross-shaped sample is stretched biaxially and symmetrically by adjusting the separation of
8
9 teeth placed in the eyelets on the ends of the arms.^{2, 13} Stretching can be quantified using the
10
11 distance X between the teeth on opposite arms of the specimen, and X_0 , which is the value of X
12
13 when no stress is applied (~ 42 mm at manufacture).^{2, 12, 13, 45} TPU (as with all elastomers) is
14
15 viscoelastic, but mechanical reproducibility can be maximised by stress-cycling.^{11, 13, 46} Macroscopic
16
17 membrane actuation changes the micro- or nanoscale pore geometry and ionic resistance, and these
18
19 relationships have been modelled both empirically^{11-13, 47} and using finite element approaches.^{13, 45}
20
21 Models for stretching^{13, 45, 47} have been used to calculate membrane thickness in experiments.^{2, 8, 41, 48}
22
23 Membrane thickness can be measured using confocal images^{3, 43} or a modified micrometre screw
24
25 gauge.^{6, 7, 10, 47}
26
27
28
29
30

31 The commercial *qNano* instrument (Izon Science, Figure 1(c))² builds on earlier TRPS apparatus.^{1, 11, 12}
32
33 Precise application of pressure across the membrane controls pressure-driven liquid flows through a
34
35 pore, and this is enabled by the gravitational pressure head of water within a variable pressure
36
37 manometer (VPM),⁸ along with knowledge of the inherent pressure head in the fluid cell.^{6, 7} Signal
38
39 noise and bandwidth are important,²⁹ and undersampling occurs if particles are driven too quickly
40
41 through a pore, causing the pulse duration to approach the 50 kHz sampling rate.³⁸ The *qViro*
42
43 apparatus (Izon Science) uses the same specimen type, and can withstand the decontamination
44
45 processes required for experimentation with viruses. Further bespoke developments (*e.g.* high
46
47 frequency actuation⁴⁶ and co-ordination with optical techniques⁴⁹) can be anticipated.
48
49
50
51
52

53 **Analysis and measurement protocols**

54
55 Simple, efficient resistive pulse analysis is necessary for high-throughput experimentation. Here we
56
57 briefly introduce physical modelling that has been used to develop TRPS protocols for measuring
58
59
60

1
2
3 particle concentration, size, and charge. In the regime relevant to TRPS, models are typically
4
5 constructed by calculating resistive pulse magnitude as a function of particle position, and separately
6
7 calculating the motion of a particle by considering transport mechanisms acting upon it. Separation
8
9 of these calculations is justified by the relatively small timescale of ionic diffusion.⁵⁰
10

11
12
13 A semi-analytic technique has been used to calculate resistive pulse size as a function of particle
14
15 position in TRPS,⁵¹ based on previous RPS work.^{9, 11} Early analyses for cylindrical^{15, 52} and conical²⁷
16
17 pores suggest that the pore's electrical resistance to ionic current R_0 can take the form
18
19

$$20$$

$$21$$

$$22 R_0 = \int \frac{\rho}{A(z)} dz, \quad (1)$$

$$23$$

$$24$$

$$25$$

$$26$$

27 where $A(z)$ is the pore's cross sectional area at position z (Figure 1(a)). Here it is assumed that the
28
29 electrolyte resistivity ρ is homogeneous, because the size of the electrical double layer (EDL, *e.g.*
30
31 ranging between 10 to 1 nm for 1 to 100 mM KCl) is small relative to usual TRPS geometry. The
32
33 access resistance beyond the ends of the pore⁵³ ($R_{end} = \rho / 4a$ for opening radius a) is usually
34
35 included.² If a particle (an insulating sphere) is introduced, the new pore resistance can be
36
37 numerically calculated using the same approach. By implementing this technique, models^{43, 51} have
38
39 reproduced experimental resistive pulse asymmetry, enabled resistance calculations when a particle
40
41 is partly or fully outside of the pore, and found that pulse size should be maximised when the
42
43 particle is not entirely within a conical pore.^{44, 53}
44
45
46
47

48
49 The particle position as a function of time can be calculated using the Nernst-Planck approach.⁵⁴
50

51 Transport mechanisms give a vector sum for the particle flux \mathbf{J} (units: particles $\text{m}^{-2} \text{s}^{-1}$), taking the
52
53 form
54

$$55$$

$$56$$

$$57 \mathbf{J} = (\mathbf{J}_{ep} + \mathbf{J}_{eo}) + \mathbf{J}_{pdf} + \dots$$

$$58$$

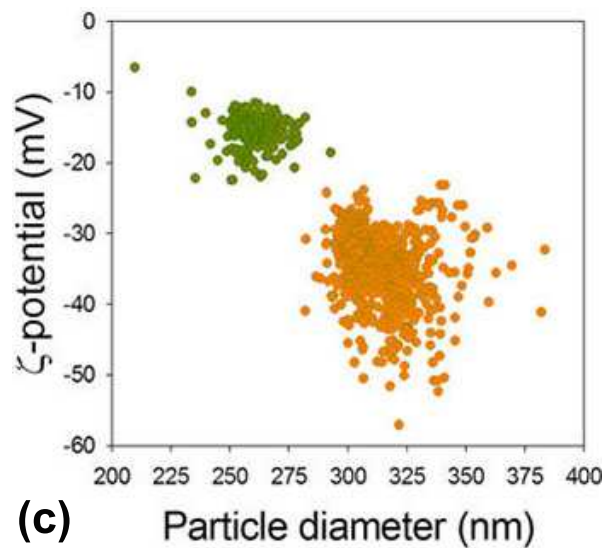
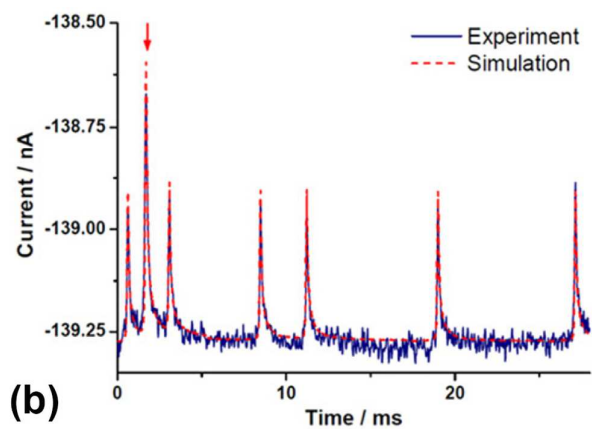
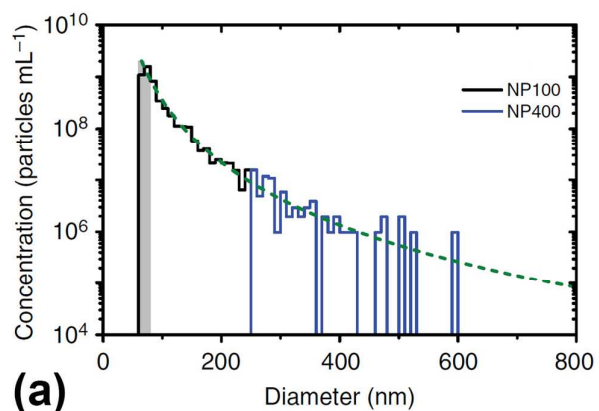
$$59$$

$$60$$

$$= \frac{C\varepsilon}{\eta} (\zeta_{particle} - \zeta_{pore}) \mathbf{E} + \frac{C\mathbf{Q}}{A} + \dots \quad (2)$$

The specified terms represent fluxes driven by the three most important mechanisms for TRPS: electrophoresis (\mathbf{J}_{ep}), electro-osmosis (\mathbf{J}_{eo}) and pressure-driven flow (\mathbf{J}_{pdf}). C , ε and η are respectively particle concentration, solution permittivity and viscosity. ζ is the zeta potential of the subscripted surface, \mathbf{E} is the electric field and \mathbf{Q} is the volume flow rate. The explicit expressions for electrophoresis and electro-osmosis are appropriate for a thin EDL, and all three terms require that the pore wall has a low gradient, approximating a cylinder.^{7, 54} Development of transport modelling for TRPS was recently summarized, with the relative importance of transport mechanisms compared over a range of geometries.⁵⁵ Together, Eqs. 1 and 2 can be used to construct resistive pulses.^{6, 43, 48} The model developed for TRPS has been used elsewhere,⁵⁶ and there are relevant RPS studies of transport mechanisms.^{22, 34, 57} Finite element modelling of TRPS^{51, 58} has used comparable methodologies to conical-pore RPS simulations,^{32, 40, 50, 59} and has been compared with the semi-analytic model.⁵¹

Concentration. When transport is dominated by pressure-driven flow, the pulse rate is proportional to the flow rate and independent of chemical and physical differences between particles (Eq. 2). Concentration of an unknown particle set can be calculated by calibrating the pressure-driven flow using particles of known concentration. Using standard PS particles, the pulse rate has been demonstrated to vary linearly with pressure up to $\sim 1.8 \text{ kPa}^{2, 5}$ and with concentration between approximately 1×10^8 and $5 \times 10^{10} \text{ mL}^{-1}$.^{2, 4, 44} Independence from particle type has been confirmed by verifying these relationships with particles such as virions and bacteria,^{4, 44, 60} and liposomes.⁶¹ Alternative concentration methods include a calibration-free method using geometric parameters^{4, 44} and an internal calibration technique⁶² which avoids the requirement for separate sample and calibration measurements and could therefore be advantageous for complex biological media.



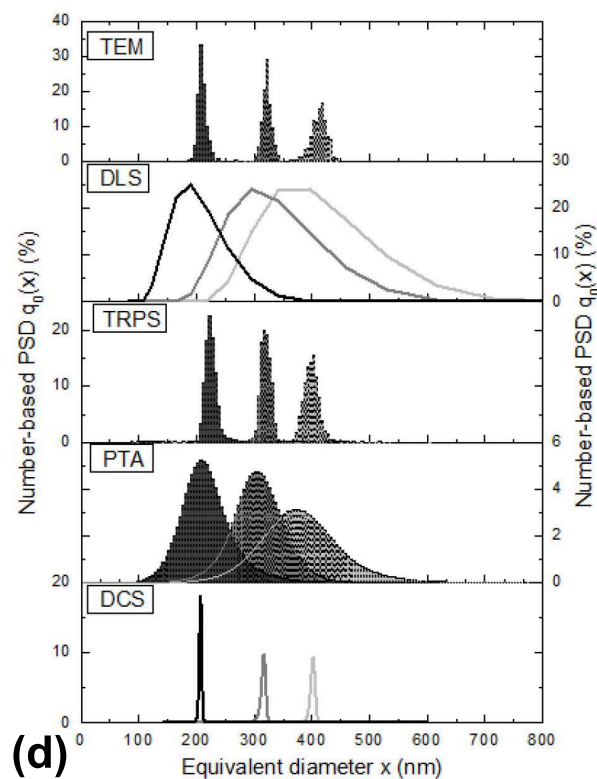


Figure 2: Analysis and measurement. (a) Size distributions for urinary EVs obtained using two tunable pores of different size (black and blue data) are combined to give a wide-ranging distribution, fitted by power law (green dashes). Reproduced from van der Pol *et al.*⁶³ (b) Resistive pulses for 1 μm spheres from an experiment (blue) and the semi-analytic model (red). The pulse indicated by the red arrow is modelled as a dimer of spheres, whereas other pulses correspond to individual particles. Reproduced from Willmott *et al.*⁴⁸ (c) Two populations of 300 nm carboxylated PS particles are distinguished from a mixture. The scatter plot includes particle-by-particle measurements of size and ζ_{particle} , the latter calculated from FWHM durations. Reprinted with permission from Kozak *et al.*, *ACS Nano*, 2012, **6**, 6990.⁶ Copyright 2012 American Chemical Society. (d) Comparison of TRPS with other particle characterization techniques (PTA is equivalent to NTA) showing PS particle size distributions for three solutions. Reproduced from Anderson *et al.*⁶⁴

Size. The principle that particle volume is proportional to the corresponding pulse magnitude was established using cylindrical pores¹⁵ and first demonstrated with TRPS by Vogel *et al.*,³ who also

1
2
3 showed that results were consistent with the semi-analytic model (based on Eq. 1) for conical pores.
4
5 TRPS size measurements have been carried out at a range of pore stretch settings,⁴⁷ using multi-
6
7 modal distributions,^{44, 62-64} and by combining size distributions obtained using pores of different sizes
8
9 (Figure 2(a)).⁶³ Arjmandi *et al.* recently used TRPS apparatus to demonstrate a sedimentation
10
11 technique for nanoparticle mass measurement,⁶⁵ citing the need for new mass measurement
12
13 methods for virions in particular.
14
15

16
17
18 Particles are usually assumed to be spherical for analysis, and in this Review sizes refer to the
19
20 equivalent spherical diameter (unless stated). However, the semi-analytic model can be applied to
21
22 any smooth functions describing pore and particle geometry. TRPS of non-spherical particles is
23
24 gaining prominence, with recent examples including self-assembled cylinders,⁶⁶ viruses,²¹ bacterial
25
26 chains,⁶⁰ and specific aggregates.⁶⁷ Particle aggregates are especially important for assays, in which a
27
28 target molecule causes two or more particles to stick together. Two recent assays^{68, 69} have
29
30 attributed pulses to dimers, trimers, and tetramers when the pulse height has been an integer
31
32 multiple of the height for individual particles, as initially modelled for superparamagnetic particle
33
34 aggregates (Figure 2(b)).^{48, 67}
35
36
37
38
39

40 **Charge.** TRPS can be used to find a particle's zeta potential (ζ_{particle}), the most widely used measure
41
42 of colloidal electronic charge. Considering Eq. 2, the electrophoretic mobility can be calculated by
43
44 measuring the particle velocity, then finding the electric field and pressure-driven flow using the
45
46 semi-analytic model. To enable calculation of ζ_{particle} , the zeta potential of TPU (ζ_{pore}) has been
47
48 measured.^{7, 42} TRPS measurement of ζ_{particle} was first achieved⁷ by finding the pressure at which $\mathbf{J} = 0$
49
50 in Eq. 2. Pressure can be varied either continuously or in discrete steps, and $\mathbf{J} = 0$ can be identified
51
52 using either the greatest value of the full-width half maximum (FWHM) duration or the minimum
53
54 pulse rate.⁴² When \mathbf{J} is non-zero, velocity profiles can be built for individual pulses,⁴⁷ yielding particle-
55
56 by-particle ζ_{particle} values using either geometric inputs⁶ (Figure 2(c)) or calibration particles.⁸
57
58
59
60

1
2
3 Comparable RPS charge measurements include a method based on transit time alone²⁴ as well as
4
5 more detailed calculations.^{22,38} TRPS has been used to find ζ_{particle} for an emulsion,⁴¹ liposomes^{70,71}
6
7 and DNA conjugated nanoparticles.⁷² Pulse rates and durations can also be used to infer changes in
8
9 surface functionalization without explicit calculation of charge.^{2,44,73-76} For example, injectable drug
10
11 carriers often use poly(ethylene glycol) (PEG) to avoid adhesion to biological material before
12
13 reaching a tumour, and TRPS can be used to observe the addition of PEG to particle surfaces.⁷⁷
14
15

16 17 18 **Ongoing technical development**

19
20 At present, the greatest measurement uncertainties when using the semi-analytic model usually
21
22 relate to pore geometry, and interactions driven by steric factors or surface chemistry.⁷⁸ Brownian
23
24 motion can generate complicated pulse shapes when particles are slow-moving¹⁰ or comparable in
25
26 size to the pore opening.⁷⁹ The importance of particle trajectory has become evident due to spatial
27
28 variations both along^{42,51} and perpendicular to⁵⁵ the pore axis. The effects and potential uses of
29
30 additional transport mechanisms could be studied, including dielectrophoresis,⁵⁵ diffusion-osmosis⁸⁰
31
32 and thermophoresis.⁸¹ Zeta-potential measurements will become more widely applicable following
33
34 collection of more ζ_{pore} and calibration ζ_{particle} data under different experimental conditions. Ionic
35
36 distributions can cause resistive pulse distortions in relatively low molarity electrolyte,^{50,82,83} and
37
38 could be explored in more detail using the Poisson-Nernst-Planck (PNP)⁵⁰ or space-charge^{54,82,84}
39
40 continuum models.
41
42
43
44
45

46 47 **Comparison with other techniques**

48
49 Colloidal characterization techniques such as TRPS, dynamic light scattering (DLS)⁸⁵ and scanning and
50
51 transmission electron microscopy (SEM and TEM) each employ different physical principles. They are
52
53 often used together to study the same sample, with each experiment providing distinct information.
54
55 Two quantitative studies^{64,86} have compared the same emerging techniques (TRPS, nanoparticle
56
57 tracking analysis (NTA), and differential centrifugal sedimentation (DCS)) with more established
58
59
60

1
2
3 techniques (TEM and DLS). Anderson *et al.*⁶⁴ measured particle size distributions for monodisperse
4
5 and multiple population solutions of 220-410 nm PS particles (Figure 2(d)), whereas Bell *et al.*,⁸⁶ who
6
7 also used scanning mobility particle sizing (SMPS), measured monodisperse samples of five Stöber
8
9 silica particle sets with diameters of 100-400 nm. Both studies produced TRPS size distributions
10
11 consistent with TEM. Another quantitative comparison⁶³ included multimodal size distributions of PS
12
13 beads measured alongside urinary EVs, and compared TRPS with TEM, NTA, and conventional and
14
15 dedicated flow cytometry (FC). For the PS beads (> 100 nm), TRPS had the lowest sizing error after
16
17 TEM and dedicated FC, with the latter technique performing well due the refractive index uniformity
18
19 of PS particles. In concentration measurements (approximate range 10^9 - 10^{10} mL⁻¹), TRPS gave good
20
21 results for PS standards, and results for EVs agreed with values obtained using NTA, with FC giving a
22
23 lower result and TEM suffering from losses during sample preparation. Recently, Varga *et al.*⁷⁸ used
24
25 EVs to compare TRPS, NTA, electron microscopy, small angle X-ray scattering (SAXS), size exclusion
26
27 chromatography and DLS. Modal values were consistent (~130 nm) across the techniques, but the
28
29 size distributions varied. There are similar comparative studies that have not involved TRPS.^{87, 88}
30
31
32
33
34

35 Eldridge *et al.*¹⁰ made a qualitative comparison of TRPS with DLS, NTA, DCS, FC, suspended
36
37 microchannel resonators (SMR) and electron microscopy in the context of drug delivery applications.
38
39 The physical nature of each technique was summarized, and measureable ranges of sample size,
40
41 concentration and volume were tabulated. Similar qualitative comparisons have specifically referred
42
43 to measurement of EVs⁸⁹ and solid lipid nanoparticles.⁹⁰ Heider and Metzner's review of virion
44
45 measurement methods²¹ considered TRPS, NTA, advanced field flow fractionation (FFF), and a virus
46
47 counter method involving fluorescent labelling, along with time-consuming biological techniques.
48
49 Advantages of TRPS for virions include efficient size measurement to determine aggregation state,
50
51 the ability to measure low particle concentrations by applying pressure, and (along with NTA and
52
53 FFF) charge measurement capability. Virus shape is not a great issue for TRPS, while the small
54
55 instrument footprint and the possibility for specificity are advantages. On the other hand, some
56
57
58
59
60

1
2
3 viruses are currently beyond the lower size capabilities of TRPS, and refinement of raw biological
4
5 samples is important for all techniques.
6
7

8
9
10 Other experimental comparisons involving TRPS have typically been restricted to a few
11
12 measurements, the relative merits of which may not extend beyond each set of experimental
13
14 conditions. Perceived advantages of TRPS have included the accessible ranges of particles,⁸⁶
15
16 electrolytes^{86, 91} and measured quantities.^{63, 91, 92} Advantageous sample volume (tens of μL),^{60, 93} cost
17
18 and portability⁹¹ and accuracy⁶¹ have also been noted. The accessible size range is not unlimited,^{62, 63,}
19
20 ^{86, 94 78} but can be extended by the use of multiple pores. Discussions of measurement speed (a few
21
22 minutes per measurement, following training)^{60, 63} and associated pore clogging⁶³ require
23
24 experimental context. For example, sample preparation⁹⁵ and classification is an issue for complex
25
26 biological media regardless of the measurement technique.⁹³ In concentration measurements, TRPS
27
28 has been more accurate than flow cytometry and phase contrast microscopy,^{4, 92} and better than
29
30 than optical density measurements for matching the plating method for bacteria.⁶⁰ However,
31
32 inconsistencies have been demonstrated in a comparative study of ~ 200 nm EVs and liposomes⁷¹
33
34 and studies affected by sample contamination.^{21, 60, 96} There is relatively little comparative work
35
36 involving charge measurement. Like TRPS, commonly used DLS-based techniques derive $\zeta_{particle}$ from
37
38 electrophoretic mobility (Eq. 2). In a recent comparison using ~ 200 nm PS particles,⁴² the typical
39
40 difference between zeta potentials obtained using TRPS and DLS was 15% (< 5 mV), with an
41
42 experimental error of $\sim 10\%$ for each technique.
43
44
45
46
47

48
49 **Distinct characteristics.** TRPS avoids difficult sample preparation and experimental artefacts
50
51 associated with electron microscopy,³⁸ although the electrolyte can cause unwanted aggregation.⁹⁰
52
53 Measurements are independent of optical properties⁷⁸ such as particle labelling, knowledge of
54
55 refractive index, or refractive index contrast. TRPS analyses assume that the particle is an ideal
56
57 insulator, and measurement protocols can require calibration.⁶³ Experimental parameters can be
58
59
60

1
2
3 varied to optimize TRPS data resolution, and two recent studies have done this systematically.^{71, 97}
4
5 When particles fall outside the size detection thresholds for a particular pore, summary statistics⁹⁷
6
7 and concentration measurements^{71, 97} are necessarily affected. This highlights the advantage of using
8
9 the mode to describe particle size distributions, and the benefits of TRPS comparisons under
10
11 identical experimental conditions. In terms of data handling, TRPS provides particle-by-particle data
12
13 which is beneficial for resolving multi-modal^{44, 62-64} and high dispersity^{63, 90, 98} distributions (especially
14
15 in comparison with DLS), can be used to calculate any central value or spread statistic, and can be
16
17 transformed for direct comparison with ensemble average data (see Supplementary Information).⁴¹
18
19

20
21
22 Many considerations apply more generally when selecting a colloidal characterization technique. For
23
24 example, the accessible ranges of particle concentration and size is important, as well as the volume
25
26 and type of solution (for TRPS, see the Introduction). The overall importance of user knowledge
27
28 regarding instrument settings and data handling has been noted.^{71, 78} Care is required regarding the
29
30 specific type of size measurement⁸⁶ and theoretical differences in size distributions.^{63, 87} For
31
32 biological solutions, sample preparation is especially critical. Lane et al.'s⁹⁵ TRPS study, which used
33
34 liposomes to systematically compare isolation protocols based on ultracentrifugation, sedimentation
35
36 reagents and density gradient, is important in this respect. There are opportunities to develop
37
38 traceable uncertainty analyses for most emerging techniques, including TRPS.⁷⁸ Coumans et al.⁹⁷
39
40 recently used TRPS to obtain 102 repeat size distribution measurements for urinary vesicles,
41
42 highlighting the importance of studying reproducibility. Finally, the experimental design should
43
44 always be considered relative to the specific research question.
45
46
47
48
49
50
51
52
53
54
55
56
57
58
59
60

Table 1. Summary of TRPS studies in which particle aggregation has been detected. PEG = poly(ethylene glycol), PDGF = platelet-derived growth factor, PNA = peptide nucleic acid, SPBs = superparamagnetic beads, RBCs = red blood cells.

| Ref. | Particle Material | Surface Function | Indicative Size ¹ / nm | Particle Concentration / $\times 10^9 \text{ mL}^{-1}$ | Analyte | Analyte Concentration ² | Detection |
|---------------|-------------------|---------------------------|-----------------------------------|--|--------------------|------------------------------------|---|
| Assays | | | | | | | |
| 67 | Au/Ni rods | Avidin (Ni) and PEG (Au) | 1230 long x 300 diameter | 0.24 | Biotin | ~100 fM | Mean ΔI , FWHM |
| | | Aptamer (Ni) and PEG (Au) | 1100 long x 300 diameter | 0.09 | PDGF | ~100 fM | Mean ΔI , FWHM |
| 68 | SPBs | Avidin | 3000 | 0.5 | Biotin | ~1 pM – 1 nM | Mean ΔI , mono- and multimer fractions |
| | | Avidin | 1000 | 6 | Biotin | ~1 nM | Monomer fraction |
| | | Streptavidin | 300 | 10 | Biotin | ~1 nM | Monomer fraction |
| 69 | Au | DNA ³ | 25 | 60 | DNA | 5.0 pM | Pulses observed |
| 73 | Au | Citrate | 50 | 45 | PNA | 5 nM | Size-duration scatter plot |
| 99 | Au | (i) Avidin (ii) DNA | (i) 30 (ii) 55 | (i) 4.2 (ii) 13 | DNA | 530 copies | Size threshold |
| 100 | Magnetic beads | Protein ⁴ | 1000 | 6×10^{-4} | RBCs | ~ 10^7 mL^{-1} | Mean size, size distribution |
| Other | | | | (Specified units) | (Mechanism) | | |
| 41 | Soy bean oil | β -lactoglobulin | 150 | 10 wt% oil | ~120 days | | Size mode, mean |
| | | β -lactoglobulin | 150 | 10 wt% oil | Salt | | Size mean, median |
| 48 | SPBs | Carboxylate | 1000 | $0.4 \times 10^9 \text{ mL}^{-1}$ | Bar magnet | | Size distribution, pulse rate, time between pulses ⁵ |
| 91 | Carbon Nanohorns | | 1-2 | $0.5\text{-}50 \mu\text{g mL}^{-1}$ | In cell media | | Size distribution |
| | Carbon black | | 14 | $0.5\text{-}50 \mu\text{g mL}^{-1}$ | In cell media | | Size distribution |
| | CeO ₂ | | 7-25 | $0.5\text{-}50 \mu\text{g mL}^{-1}$ | In cell media | | Size distribution |
| | Ni | | 60 | $0.5\text{-}50 \mu\text{g mL}^{-1}$ | In cell media | | Size distribution |
| 101 | Liposomes | EPC-3-based ⁶ | 250 | 5 mM lipids | ~1 hr | | Size distribution |
| 102 | Wine proteins | | 200 – 4000 ⁷ | 100 mg L ⁻¹ | Heating | | Size distribution, concentration |

¹ As available: mode, mean or manufacturer's specification.

² Order of magnitude estimate indicated by ~ unless limit of detection claimed in original publication.

³ Two types of bead with different DNA ends (18 and 100 bp) matching the ends of the target.

⁴ The protein annexin-V binds to phosphatidylserine found on the surface of RBCs after eryptosis.

⁵ This study pointed out that the mean particle size gives higher sensitivity to aggregation than the mode when most beads are not aggregated.

⁶ Hydrated egg phosphatidylcholine in lipolysis medium.

⁷ Range of aggregate sizes formed from molecular protein.

Applications

Diagnostics and Genomics

This section focusses on the use of TRPS to study DNA, aptamers and other molecules which support specific binding interactions. The goal is often a diagnostic, sensing or monitoring assay at low concentrations of target. Bead aggregation is one common method for detecting the presence of a target, and understanding particle aggregation is of wider importance for TRPS. TRPS studies of particle aggregation have been summarised in Table 1.

DNA. As noted in the Introduction, interest in the wider field of nanopore science has been driven by potential DNA sensing applications. TRPS is no exception, as the first description of size-tunable pores¹ involved detection of dsDNA molecules each consisting of 2686 base pairs (bp). Controlled gating of these molecules was reported (Figure 3(a)), with resistive pulses observed only at relatively high stretch. The particular geometry of the pore used in this study allowed detection of DNA molecules, but due to the relative ease of tunable pore fabrication at larger length scales, no subsequent TRPS studies have reported detection of single molecules.

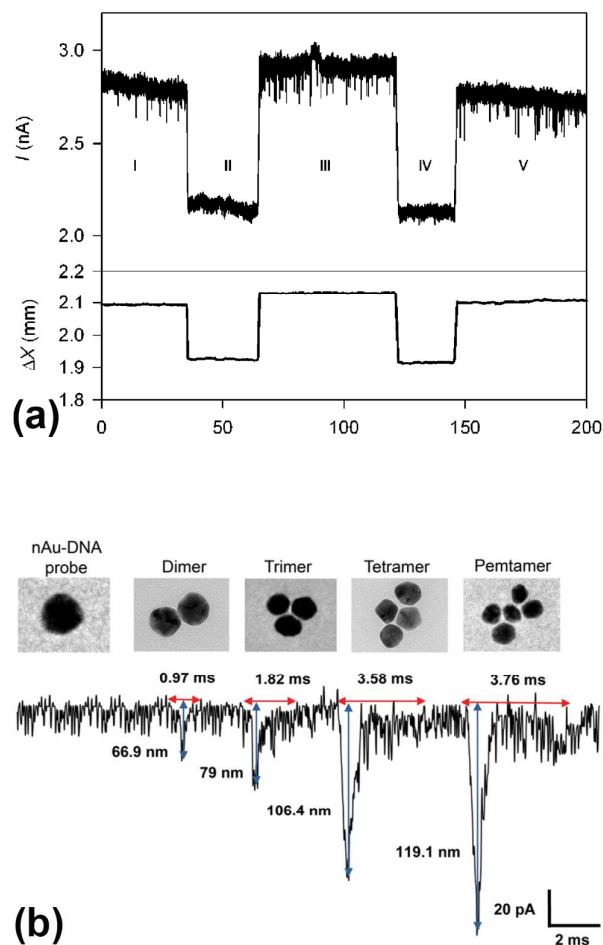


Figure 3: TRPS experiments using DNA. (a) Gating of 2.7 kbp dsDNA molecules, reproduced from Sowerby *et al.*¹ Traces show the stretch applied to a membrane (lower), and ionic current (upper) as a function of time. Zones labelled I-V are delineated by abrupt changes corresponding to adjustment of ΔX . (b) Distinguishing multimers of DNA-aggregated 25 nm Au nanoparticles. TEM images (upper) demonstrate aggregates as observed in the ionic current trace (lower). Arrows and labels indicate the mean baseline duration and modal magnitude. The latter is scaled to effective spherical diameter. Reprinted with permission from Ang and Yung, *ACS Nano*, 2012, **6**, 8815.⁶⁹ Copyright 2012 American Chemical Society.

Subsequently, TRPS has been used for on-bead DNA sensing in which evidence for molecular interactions is provided by detecting changes in particle size or surface charge due to functionalization or aggregation. Firstly, TRPS was used to simply distinguish 220 nm organosilica

1
2
3 nanoparticles modified with λ -DNA (48 kbp dsDNA, ~ 16 nm long) from unmodified particles.⁴⁴ The
4
5 modified particles produced an increased pulse duration resulting from reduced surface charge,
6
7 without an observable increase in particle size. Low *et al.* studied non-specific aggregation of citrate
8
9 capped gold nanoparticles in the presence of a mixed base peptide nucleic acid (PNA, 20 bp
10
11 ssDNA).⁷³ The TRPS size measurement for single nanoparticles (~ 50 nm) agreed with DLS and TEM
12
13 results. On addition of PNA, TRPS indicated aggregates with diameters up to 125 nm in addition to
14
15 charge neutralisation (increased pulse duration). The lowest PNA concentration at which
16
17 aggregation was inferred was 5 nM, whereas 50 nM was required using DLS. Specific DNA
18
19 interactions were first studied with TRPS by Booth *et al.*,⁷² who functionalized dextran-based
20
21 magnetic beads with 23 bp DNA complementary to a target. There was no significant change in the
22
23 modal size recorded before (109 nm) and after (106 nm) the addition of 0.01 nM target DNA to $2 \times$
24
25 10^{11} mL⁻¹ beads, but the modal FWHM duration was reduced from 0.95 ms to 0.68 ms. This
26
27 indication of increased particle charge was verified using TRPS charge measurements⁷ in which the
28
29 zeta potential increased from -11 mV to -17 mV.
30
31
32

33
34
35 Two studies^{69,99} have used a TRPS sensing strategy in which two types of gold nanoparticle have
36
37 induced aggregation in the presence of specific target DNA. In both cases individual nanoparticles
38
39 were too small to be detected, so resistive pulses indicated the presence of the target. Ang and
40
41 Yung⁶⁹ prepared two sets of 25 nm gold particles with DNA fragments (18 and 100 bp)
42
43 complementary to the different ends of a target. With the target present, the observed aggregates
44
45 could be classified as dimers, trimers, tetramers and pentamers on the basis of pulse magnitudes
46
47 (Figure 3(b), see also⁶⁸). Aggregates were not observed when the target sequence was altered by a
48
49 single base. Target concentrations from 5.0 pM to 2.5 nM were near-linearly correlated with
50
51 aggregate detection rate, suggesting a method for quantifying target DNA concentration. Yang *et*
52
53 *al.*⁹⁹ used 30 nm and 55 nm gold nanoparticles functionalized with avidin and a thiol-DNA probe
54
55 respectively. The target DNA, a 340 bp gene from methicillin-resistant *Staphylococcus aureus*
56
57
58
59
60

1
2
3 (MRSA), underwent loop-mediated isothermal DNA amplification (LAMP) so that it would bind to
4
5 both types of nanoparticle, inducing aggregation. Using arbitrary size thresholds, the authors quoted
6
7 a limit of detection of 530 DNA copies within a processing time of 2 hours. The technique was tested
8
9 against a negative control, and also showed good specificity against a strain of *S. aureus* which does
10
11 not carry the same gene.
12

13
14
15
16 Most recently,¹⁰³ TRPS has been used for label-free counting of individual strands of synthetic *P.*
17
18 *aeruginosa* DNA. Padlock probes, which ensured specific capture of the target, were bound to 1 μm
19
20 magnetic beads and subjected to rolling circle amplification (RCA), producing large coils of ssDNA
21
22 attached to the beads. When beads were mixed with DNA at a 10:1 ratio, the number of strands
23
24 could be quantified using the increased baseline pulse duration. This method was demonstrated
25
26 using a pulse duration detection threshold, with a lower detection limit near to 10 zmol of DNA in 10
27
28 μL of electrolyte (*i.e.*, 1 fM). The authors noted that the method is more sensitive than similar
29
30 fluorescence based methods, with a total assay and analysis time under 1 hour.
31
32

33
34
35 **Aptamers and other specific interactions.** Aptamers are short, single-stranded pieces of DNA or RNA
36
37 that are developed to have specific binding affinity for a target molecule.⁶⁷ The selectivity, stability
38
39 and cost of aptamers is attractive for sensing applications.^{67, 74, 104} In that context, it is unsurprising
40
41 that TRPS has been used to investigate the use of aptamers more often than other specific
42
43 interactions. Platt *et al.*⁶⁷ were the first to use TRPS to study both an aptamer capture probe and the
44
45 avidin-biotin interaction. The detection strategy involved aggregation of cylindrical nanorods
46
47 (diameter 300 nm, length 2-4 μm) in the presence of the target protein, platelet-derived growth
48
49 factor. Each rod was a 'barcode' of gold and nickel segments. By appropriate functionalization of the
50
51 barcode, the orientation of aggregates could be controlled, and changes in pulse magnitude and
52
53 FWHM were specific to the resulting aggregate shape (Figure 4(a)). Detection in the femtomolar
54
55 range was enabled by the superparamagnetic properties of the Ni-containing rods.
56
57
58
59
60

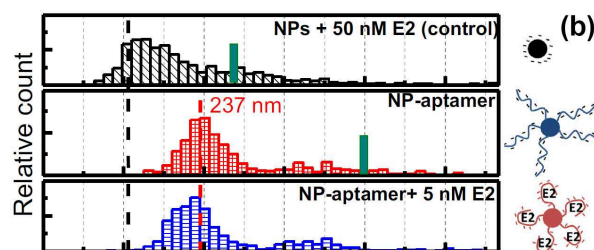
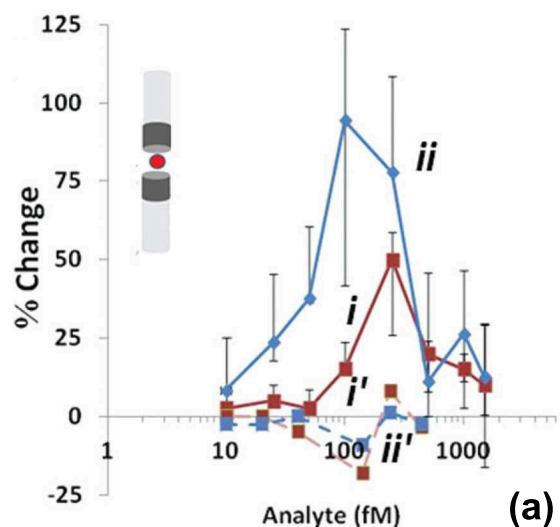


Figure 4: TRPS experiments using aptamers and the avidin-biotin interaction. (a) Nanorod aggregation in the presence of BBSA. Only the Ni segments of AuNi barcoded rods (dark grey in inset schematic) were functionalized with avidin, inducing end-to-end aggregates. The changes in resistive pulse magnitude (i, red) and FWHM duration (ii, blue) are compared with a control analyte (dashed lines). Reproduced from Platt *et al.*⁶⁷ (b) TRPS size histograms with accompanying schematic diagrams for carboxylated PS nanoparticles in the presence of a target (upper), the same nanoparticles coupled to aptamers (middle), and modified nanoparticles with the target present (lower). Black and red dashed lines indicate the modes of the upper and middle distributions respectively, and green bins indicate the average of DLS size distributions. Adapted from Alsager *et al.*⁷⁴

1
2
3 Billinge *et al.*⁶⁸ subsequently used TRPS to study aggregation of 3 μm superparamagnetic beads
4 coated with avidin in the presence of picomolar biotinylated bovine serum albumin (BBSA).
5
6 Aggregation, as indicated by increased pulse sizes and fewer pulses, reduced at higher analyte
7 concentrations (~ 1 nM) due to saturation of the bead surface with analyte. This 'hook' effect, so-
8 called because of the form of data plots, can produce a false negative result and is a general feature
9 of aggregation assays. This assay was also studied with variations in bead concentration, bead size,
10 binding capacity, and with a bar magnet present. The same team reported on detection of the
11 protein thrombin using beads modified with three different aptamers.¹⁰⁴ In this study, the decrease
12 in pulse rate due to charge screening was the best indicator of target presence, and pulse rates were
13 studied in real time (over ~ 3 minutes) after thrombin (0.1-1000 nM) was added to the beads (3×10^9
14 mL^{-1}) in the TRPS fluid cell. The change in pulse rate allowed calculation of dissociation constants for
15 the aptamers, and the values obtained were consistent with literature. Variations in assay
16 performance between the three aptamers were attributed to conformational changes when binding
17 to the target.
18
19
20
21
22
23
24
25
26
27
28
29
30
31
32
33
34

35 Alsager *et al.* also used an on-bead aptamer based detection strategy, but without aggregation.⁷⁴ An
36 aptamer for the target 17 β -estradiol was tethered to 217 nm PS nanoparticles, and TRPS was used to
37 study functionalized nanoparticles (5.2×10^{10} mL^{-1}) exposed to target concentrations between 5-150
38 nM. Resistive pulse sizes increased with the attachment of the aptamer, then decreased on addition
39 of the target due to conformational change (Figure 4(b)), in qualitative agreement with DLS.
40 Nanoparticle functionalization resulted in increased pulse duration, which was inconsistent with DLS
41 charge measurements, and was attributed to increased steric drag in the pore constriction. Pulse
42 FWHM values also increased when the target was added, in agreement with the DLS trend, and
43 consistent with charge screening by the target. The assay did not discriminate between the target
44 and compounds from the same steroid family, but excellent discrimination was observed for
45 bisphenol compounds. Overall, TRPS assays using aptamers have revealed that changes in particle
46
47
48
49
50
51
52
53
54
55
56
57
58
59
60

1
2
3 size and charge can be detected, but are not always predictable due to the unique three-
4
5 dimensional binding conformation between the aptamer and its target.
6
7

8
9
10 Further specific interactions studied using TRPS include detection of aggregates formed by 1 μm
11 beads and red blood cells (RBCs).¹⁰⁰ Aggregation was enabled by the specific affinity between a
12 protein on the beads and the outer lipid bilayer of RBCs following eryptosis, which was instigated
13 either by increasing osmolarity or using a potential anti-cancer drug. Lai *et al.*¹⁰⁵ used TRPS size
14 distributions to observe binding of antibody-loaded protein microparticles to a target molecule.
15 Protein microparticles were suspended in the fluid cell above a pore, and the mean particle diameter
16 increased from 1041.5 nm to 1212.6 nm when the target (mouse IgG) was introduced. No size
17 change was observed on the addition of rabbit IgG.
18
19
20
21
22
23
24
25
26
27

28 **Extracellular vesicles**

29
30 TRPS is being applied widely to studies of extracellular vesicles (EVs),¹⁰⁶ which are lipid bilayer
31 vesicles secreted by most human cells. EVs play a role in inter-cell communication, in gene delivery
32 and as disease biomarkers.^{62, 106, 107} Their concentration and composition can be altered by
33 pathological conditions,¹⁰⁷ and they can carry microRNA (miRNA).¹⁰⁸ There is currently a need to
34 classify and understand the roles of particular EVs. By one definition,^{107, 109} EVs of endosomal origin
35 are termed exosomes (generally 30-100 nm), whereas EVs originating from the plasma membrane
36 are termed microvesicles (100-1000 nm). EVs are also sometimes referred to as microparticles.
37
38 However, classification is challenging, because a raw sample of bodily fluid (*e.g.* blood, urine or
39 lymph) contains a complex, high dispersity mixture of sub-cellular particles and proteins. This
40 problem has produced high demand for new measurement tools,⁸⁷ and consequently TRPS has
41 recently featured in several reviews and comparisons of EV measurement techniques.^{63, 78, 89, 93, 97, 110,}
42
43
44
45
46
47
48
49
50
51
52
53
54
55
56
57
58
59
60
61
62
63
64
65
66
67
68
69
70
71
72
73
74
75
76
77
78
79
80
81
82
83
84
85
86
87
88
89
90
91
92
93
94
95
96
97
98
99
100
101
102
103
104
105
106
107
108
109
110
111
112
113
114
115
116
117
118
119
120
121
122
123
124
125
126
127
128
129
130
131
132
133
134
135
136
137
138
139
140
141
142
143
144
145
146
147
148
149
150
151
152
153
154
155
156
157
158
159
160
161
162
163
164
165
166
167
168
169
170
171
172
173
174
175
176
177
178
179
180
181
182
183
184
185
186
187
188
189
190
191
192
193
194
195
196
197
198
199
200
201
202
203
204
205
206
207
208
209
210
211
212
213
214
215
216
217
218
219
220
221
222
223
224
225
226
227
228
229
230
231
232
233
234
235
236
237
238
239
240
241
242
243
244
245
246
247
248
249
250
251
252
253
254
255
256
257
258
259
260
261
262
263
264
265
266
267
268
269
270
271
272
273
274
275
276
277
278
279
280
281
282
283
284
285
286
287
288
289
290
291
292
293
294
295
296
297
298
299
300
301
302
303
304
305
306
307
308
309
310
311
312
313
314
315
316
317
318
319
320
321
322
323
324
325
326
327
328
329
330
331
332
333
334
335
336
337
338
339
340
341
342
343
344
345
346
347
348
349
350
351
352
353
354
355
356
357
358
359
360
361
362
363
364
365
366
367
368
369
370
371
372
373
374
375
376
377
378
379
380
381
382
383
384
385
386
387
388
389
390
391
392
393
394
395
396
397
398
399
400
401
402
403
404
405
406
407
408
409
410
411
412
413
414
415
416
417
418
419
420
421
422
423
424
425
426
427
428
429
430
431
432
433
434
435
436
437
438
439
440
441
442
443
444
445
446
447
448
449
450
451
452
453
454
455
456
457
458
459
460
461
462
463
464
465
466
467
468
469
470
471
472
473
474
475
476
477
478
479
480
481
482
483
484
485
486
487
488
489
490
491
492
493
494
495
496
497
498
499
500
501
502
503
504
505
506
507
508
509
510
511
512
513
514
515
516
517
518
519
520
521
522
523
524
525
526
527
528
529
530
531
532
533
534
535
536
537
538
539
540
541
542
543
544
545
546
547
548
549
550
551
552
553
554
555
556
557
558
559
560
561
562
563
564
565
566
567
568
569
570
571
572
573
574
575
576
577
578
579
580
581
582
583
584
585
586
587
588
589
590
591
592
593
594
595
596
597
598
599
600
601
602
603
604
605
606
607
608
609
610
611
612
613
614
615
616
617
618
619
620
621
622
623
624
625
626
627
628
629
630
631
632
633
634
635
636
637
638
639
640
641
642
643
644
645
646
647
648
649
650
651
652
653
654
655
656
657
658
659
660
661
662
663
664
665
666
667
668
669
670
671
672
673
674
675
676
677
678
679
680
681
682
683
684
685
686
687
688
689
690
691
692
693
694
695
696
697
698
699
700
701
702
703
704
705
706
707
708
709
710
711
712
713
714
715
716
717
718
719
720
721
722
723
724
725
726
727
728
729
730
731
732
733
734
735
736
737
738
739
740
741
742
743
744
745
746
747
748
749
750
751
752
753
754
755
756
757
758
759
760
761
762
763
764
765
766
767
768
769
770
771
772
773
774
775
776
777
778
779
780
781
782
783
784
785
786
787
788
789
790
791
792
793
794
795
796
797
798
799
800
801
802
803
804
805
806
807
808
809
810
811
812
813
814
815
816
817
818
819
820
821
822
823
824
825
826
827
828
829
830
831
832
833
834
835
836
837
838
839
840
841
842
843
844
845
846
847
848
849
850
851
852
853
854
855
856
857
858
859
860
861
862
863
864
865
866
867
868
869
870
871
872
873
874
875
876
877
878
879
880
881
882
883
884
885
886
887
888
889
890
891
892
893
894
895
896
897
898
899
900
901
902
903
904
905
906
907
908
909
910
911
912
913
914
915
916
917
918
919
920
921
922
923
924
925
926
927
928
929
930
931
932
933
934
935
936
937
938
939
940
941
942
943
944
945
946
947
948
949
950
951
952
953
954
955
956
957
958
959
960
961
962
963
964
965
966
967
968
969
970
971
972
973
974
975
976
977
978
979
980
981
982
983
984
985
986
987
988
989
990
991
992
993
994
995
996
997
998
999
1000

1
2
3 extend to the smallest EVs^{78, 97} as noted in comparisons with electron microscopy (Figure 5(a)).^{62, 94,}
4
5 ¹¹⁴ Protocols for EV collection, isolation, handling, and storage for TRPS are in development,^{95, 110} and
6
7 analysis of protein content is not currently enabled.⁸⁹ The remainder of this section covers TRPS
8
9 studies of EVs isolated from particular cell types, demonstrating a wide range of measurement roles
10
11 and application areas.
12

13
14
15
16 Urinary vesicles occur naturally at relatively high concentration with low contamination. In their
17
18 comparative study, van der Pol *et al.*⁶³ used urine, centrifuged to remove cells and diluted in
19
20 phosphate buffered saline (PBS). Size distributions for these vesicles were obtained using pores of
21
22 two sizes (Figure 2(a)). Coumans *et al.*⁹⁷ also used urinary vesicles for their study of TRPS
23
24 reproducibility (see Distinct characteristics), while De Vrij *et al.*⁶² studied EVs isolated from urine as
25
26 well as blood plasma and pleural fluid. Their samples all produced TRPS size distributions with more
27
28 than 95% of particles in the range 150-400 nm. Cheng *et al.* measured size distributions for
29
30 exosomes derived from urine¹¹⁵ and blood¹¹⁴ in studies aiming to develop collection and processing
31
32 methods for miRNA sequencing. A standardized ultracentrifugation protocol was used to isolate
33
34 exosomes, and TRPS size distributions provided evidence that the miRNA yield from exosomes
35
36 isolated from urine and resuspended in PBS was superior to samples from the usual medium, cell-
37
38 free urine.
39
40
41
42
43

44 TRPS has been used to analyse the size and concentration of microparticles in blood before and after
45
46 apheresis, a treatment for removing cholesterol.¹¹⁶ Apheresis did not alter the modal microparticle
47
48 size, while the concentration dropped when measured using pores of target diameter 200 nm and
49
50 NTA, but was unchanged when using pores of target diameter 100 nm. These differences illustrate
51
52 the importance of size thresholds and sample preparation for biological fluids. Burnouf *et al.*'s
53
54 review of methods for studying platelet microparticles (PMPs),⁹³ the most abundant microparticles
55
56 in blood, included a TRPS size distribution for ~400 nm PMPs in platelet-poor plasma. PMPs are 0.1–
57
58
59
60

1
2
3 1 μm phospholipid-based fragments shed from platelets when they undergo activation, stress, or
4
5 apoptosis.
6

7
8
9 Szabó *et al.*¹¹⁷ analysed centrifuged supernatant from a culture of leukaemia cells in a study
10
11 concerned with the effects of EVs on human monocytes in the presence of recombinant human
12
13 tumour necrosis factor. As well as measuring the EV concentration and size distributions (Figure
14
15 5(b)), TRPS played a role confirming that a nominally EV-free medium was indeed free of
16
17 microvesicles. Patko *et al.*⁹⁴ obtained a size distribution in the range 200-300 nm in a study of
18
19 leukaemia-derived EVs binding to the extracellular matrix. The role of an enzyme (capase-3) in
20
21 production of EVs from breast cancer cells has also been investigated.⁹² In cells transfected with
22
23 capase-3, the concentration of EVs increased approximately 5-fold, most significantly in the size
24
25 range 400-600 nm from an overall measured range of 100-1000 nm. Here, TRPS was preferred over
26
27 FC as the latter does not give particle size information and underestimated the particle
28
29 concentration. De Vrij *et al.* also measured tumor cell-derived EVs between 100 and 200 nm in
30
31 diameter.⁶²
32
33
34
35
36

37
38 EVs derived from mesenchymal stem cells (MSCs) can be used as a delivery vehicles, and TRPS has
39
40 been used to measure size distributions for EVs that could deliver enzymes to combat Alzheimer's
41
42 disease (150-200 nm),¹¹⁸ and anti-cancer miRNA to tumour cells (60–180 nm, with the major peak at
43
44 65–75 nm).¹¹² In the latter study, TRPS suggested that the number of secreted nanoparticles
45
46 (including exosomes) increased following transfection of synthetic miRNA into MSCs. Elsewhere, EVs
47
48 from endometrial epithelial cells were compared with EVs found in uterine fluid and mucus in a
49
50 study of implantation in the uterine cavity.¹¹⁹ The similarity of size distributions from different
51
52 sources (100-500 nm with a mode of ~ 100 nm) suggested that epithelial EVs are released into the
53
54 uterine cavity. Liposomes, which are synthetic spherical compartments enclosed by a phospholipid
55
56 bilayer,¹²⁰ can be used as a model for EVs. Lane *et al.*⁹⁵ demonstrated that model liposomes had a
57
58
59
60

1
2
3 similar size distribution (~ 100 nm) to exosomes derived from serum-free cell culture media at
4
5 concentrations between 1.5×10^9 and 3×10^{11} mL⁻¹. Maas et al.⁷¹ compared analyses of tumour cell-
6
7 derived EVs and 212 nm liposomal EV mimics at 3.3×10^{13} mL⁻¹ using TRPS, NTA and high-resolution
8
9 FC. TRPS results were obtained at various pore geometries, applied voltages, buffers, calibration
10
11 particle sets and particle dilutions, and emphasized the importance of reproducible measurement
12
13 through understanding and control of experimental settings. Emerging reports on EV research¹²¹
14
15 suggest that there are other TRPS studies in progress concerning EVs derived from fibroblasts,
16
17 marrow, white blood cells, and from humans as well as animal models.
18
19
20
21
22
23
24
25
26
27
28
29
30
31
32
33
34
35
36
37
38
39
40
41
42
43
44
45
46
47
48
49
50
51
52
53
54
55
56
57
58
59
60

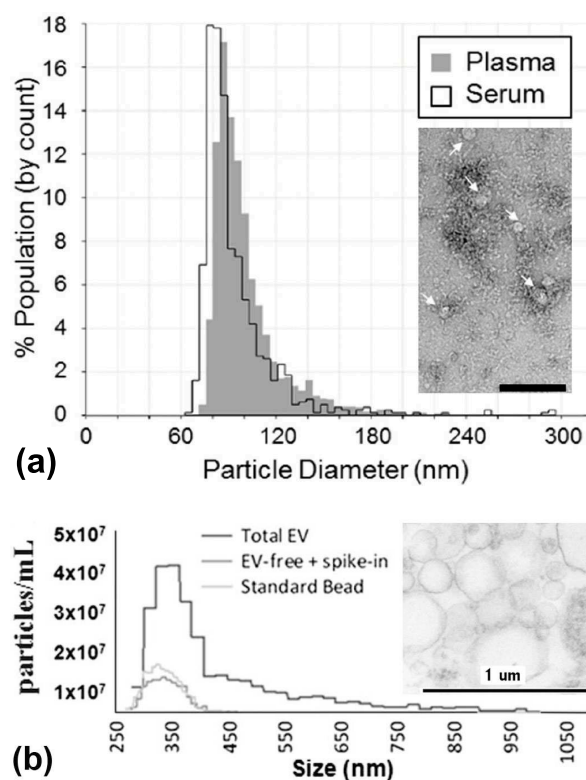


Figure 5: TRPS experiments using EVs. (a) Size distributions for exosomes from blood plasma and serum. Inset, TEM of plasma exosomes (denoted by arrows, scale bar 200 nm). Adapted from Cheng *et al.*¹¹⁴ under a Creative Commons license.¹²² (b) TRPS size distributions and TEM (inset) for EVs in cell-free supernatants derived from acute lymphoblastic leukemia cells. In the TRPS data, exclusion

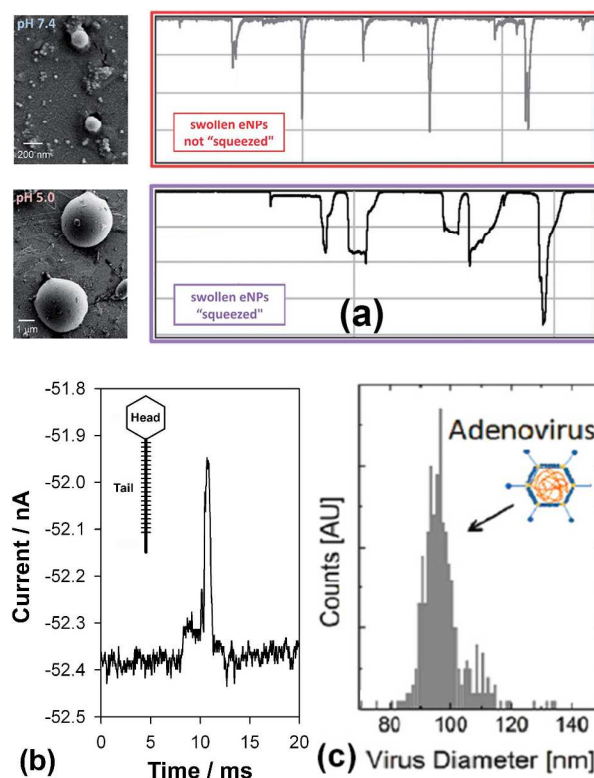
1
2
3 of EVs in one solution was confirmed by spiking the solution with 400 nm reference beads. Adapted
4
5 from Szabó *et al.*¹¹⁷
6
7

9 **Nanomedicine**

10
11
12
13
14 **Drug delivery.** Many nanoparticle formulations are being explored in order to provide new drug
15 administration methods that are non-invasive, targeted, and provide controlled medication
16 release.^{10, 123} Physical properties (including size, charge and concentration) can affect the circulation
17 time, localization, cellular uptake, drug release profile and toxicity of nanoparticles *in vivo*.¹²⁴
18 Therefore accurate characterisation is necessary to ensure effectiveness and quality control.
19
20 Regulatory compliance has been highlighted by a recent study⁷⁰ which demonstrated TRPS
21 measurement of reporting statistics for Caelyx, a commercial liposome-based drug treatment. TRPS
22 yielded a narrower size distribution than DLS, and was also used to study liposomal size differences,
23 concentration, charge (therefore surface properties), and aggregation during the freeze-thaw
24 process.
25
26
27
28
29
30
31
32
33
34
35
36

37 Liposomes, a major class of drug delivery nanoparticles, are usually prepared by extrusion of lipid
38 through a filter, producing a particle size range close to the diameter of the filter pores.^{61, 125}
39 For the first liposomes studied using TRPS,¹²⁵ particle size distributions (~200 nm) and pulse rates
40 were measured as a function of the jaw width and applied pressure. TRPS size distributions have
41 been used to monitor the stability of two liposome dispersions, by looking for signs of aggregation in
42 particle size distributions. In the first case, tumour-targeting polymer-liposome complexes (~150 nm)
43 were more stable than more standard liposome types when exposed to protein treatment.⁷⁵ In the
44 second, the size distribution of soy phosphatidylcholin (SPC) liposomes (100-160 nm) did not change
45 significantly following incubation in a medium approximating the gastro-intestinal track, whereas
46 liposomes based on hydrated egg phosphatidylcholine formed aggregates up to 1 µm in diameter
47
48
49
50
51
52
53
54
55
56
57
58
59
60

1
2
3 over 60 minutes.¹⁰¹ Yang *et al.* also studied SPC liposomes,⁶¹ extruded using filters approximately
4 100, 200 and 400 nm in size. TRPS was able to take measurements at more than 20 times greater
5 dilution of phospholipid than DLS. TRPS and DLS yielded similar size measurements for the smaller
6 two samples, while inconsistencies obtained for the largest sample were attributed to DLS
7 uncertainties caused by size dispersity. Similarly, a TRPS size distribution for lyophilisomes over the
8 range 700-1600 nm gave a mean diameter of 1214 nm,⁹⁸ in comparison with a higher DLS value of
9 1695 nm.¹²⁶ From SEM, lyophilisome size distributions are known to range in diameter from 100-
10 3000 nm. Lyophilisomes are biocapsules made from water soluble proteins, with the defining factor
11 that there is no need for amphiphilicity.¹²⁶ A method for calculating extruded liposome
12 concentrations has been tested using TRPS,¹²⁷ yielding ~90% agreement for ~200 nm liposomes at
13 ~10¹³ mL⁻¹.



54
55 Figure 6: (a) Expansive nanoparticles used for drug delivery are much larger at lower pH (SEM images,
56 left). TRPS measurements for the expanded particles (right) can 'squeeze' the particles by reducing
57
58
59
60

1
2
3 the pore size, resulting in longer pulse durations. Adapted from Ref. 74. (b) Resistive pulse for a
4
5 lambda phage (length ~230 nm), represented by the inset schematic diagram. The shoulder of the
6
7 pulse prior to the maximum resistance change suggests that the phage tail passed through the pore
8
9 prior to the head. Reproduced from Willmott *et al.*¹¹ (c) TRPS size histogram for adenovirus
10
11 particles, with inset schematic of the virus. Adapted with permission from Vogel *et al.*, *Anal. Chem.*,
12
13 2011, **83**, 3499.³ Copyright 2011 American Chemical Society.
14
15

16
17
18 Particles which release their drug in response to a particular chemical or physical stimulus are a
19
20 promising development in drug delivery. The drug can be delivered to a tumour specifically, and in
21
22 high concentrations. For example, Burgess and Porter¹²⁸ used TRPS to study phase-shift
23
24 nanoemulsions (PSNEs), which release their drug when an ultrasound stimulus converts
25
26 nanoemulsion drops to nanobubbles. The size of PSNEs (mean diameter 178.3 nm and concentration
27
28 $5.3 \times 10^{11} \text{ mL}^{-1}$) is important as they must be able to move through blood vessel walls into
29
30 neighbouring tissue. TRPS has more commonly been used to study particles which release their
31
32 payload in the slightly acidic conditions (pH 5.0) found within a cell. This is the case for ECM-
33
34 targeting liposomes (above),⁷⁵ hydrogel particles of diameter ~1500 nm which degrade below pH
35
36 7.4,¹²⁹ and polymeric nanoparticles (200-250 nm) which burst at pH 7.4 and in the presence of
37
38 gastrointestinal enzymes.¹³⁰
39
40
41
42
43

44 Colby *et al.*⁷⁹ used TRPS to study 'expansile' nanoparticles, which SEM suggests are 20-200 nm in
45
46 diameter near pH 7.4, but expand to 200-2000 nm at pH 5.0 as their polymer matrix breaks down.
47
48 The proportion of particles measured by the larger of two pores increased from <1% to 90% over 5
49
50 days, consistent with an increase of measured average diameter from $876 \pm 259 \text{ nm}$ to 1339 ± 516
51
52 nm between days 3 and 5. Pulse durations for expanded nanoparticles became larger and more
53
54 irregular when the applied stretch was decreased (Figure 6(a)), suggesting that the soft expanded
55
56 nanoparticles squeeze through the pore. This experiment represents an initial foray towards the use
57
58
59
60

1
2
3 of tunable pores to mechanically interact with soft nanoparticles, as also suggested in recent RPS
4 reports using static membranes.^{38, 131}
5
6
7

8
9
10 Magnetically loaded particles also show promise for drug delivery because they can be directed to
11 specific sites using an external magnet.¹³² TRPS has been used to measure the size distributions of
12 lipid particles that were small enough for administration by inhalation (< 5 μm), and contained
13 superparamagnetic iron-oxide nanoparticles (SPIONs) along with a model drug, budesonide.¹³³ These
14 particles had a mean diameter of 2.2 μm (mode 1.6 μm) without SPIONs, rising to 2.8 μm (mode 1.8
15 μm) when SPIONs were included. Results obtained using DLS (3.2 μm and 2.9 μm respectively) were
16 again larger due to a small population of large aggregates. The range of drug delivery systems
17 analysed using TRPS now includes solid lipid nanoparticles⁹⁰ and fluorocarbon droplets which could
18 simultaneously act as contrast agents.¹³⁴
19
20
21
22
23
24
25
26
27
28

29
30
31 **Nanotoxicology.** The potential for TRPS in nanotoxicology has been demonstrated by Pal *et al.*,⁹¹
32 who measured aggregates of engineered nanomaterials (ENMs) - carbon nanohorns, carbon black,
33 CeO₂ and Ni nanoparticles. Size and concentration measurements were carried out in fetal bovine
34 serum, and although TRPS and DLS particle size distributions were similar, TRPS was able to
35 distinguish two modes in the size distribution. A key outcome for *in vitro* toxicity assessment was
36 that particle characterization uncertainties were less significant than the uncertainty in relating an
37 administered dose to the dose delivered to a cell.
38
39
40
41
42
43
44
45
46
47

48 **Phages, viruses and bacteria**

49
50 Bacteriophages and viruses, which range in size from tens to hundreds of nanometers, and bacteria,
51 typically a few micrometers in size, can all be cultured in solutions suitable for TRPS. In these fields,
52 TRPS has mostly been used for basic characterization of size and concentration. There is a particular
53 need to complement or replace plating, the laborious gold standard for bacterial concentration
54
55
56
57
58
59
60

1
2
3 measurements.⁶⁰ The potential for TRPS in this area was first demonstrated using lambda phage,¹¹
4
5 which infects *Escherichia coli*. The shapes of resistive pulses appeared to be consistent with the
6
7 head-tail geometry of the phages (Figure 6(b)). Another phage measurement¹³⁵ concerned the
8
9 *Serratia entomophila* anti-feeding prophage (Afp), which causes amber disease in New Zealand grass
10
11 grub. A particle concentration of $4.1 \times 10^7 \text{ mL}^{-1}$ within the size range 140-165 nm was deemed to
12
13 correspond to the Afp.
14
15

16
17
18 The first TRPS measurement of a virus³ used purified samples of the spherical adenovirus virion,
19
20 suspended in PBS, yielding a size distribution with a modal value of $96.5 \pm 15 \text{ nm}$, compared with a
21
22 literature value of 70-90 nm. The narrow histogram peak (Figure 6(c)) suggested that the virions did
23
24 not aggregate, an important trait for potential gene therapy applications. Farkas *et al.*⁹⁶ used TRPS to
25
26 study rotavirus (diameter $\sim 75 \text{ nm}$), the most common intestinal virus. A size exclusion
27
28 chromatography method for sample purification was paired with TRPS to prevent virus count
29
30 overestimation, a common problem for rotavirus. On the other hand, measurements based on
31
32 protein and DNA content caused concentration overestimates ($> 10^{12} \text{ mL}^{-1}$) for lentivirus (80-100 nm)
33
34 due to contaminating molecules outside the virions.²¹ The comparative TRPS value ($8 \times 10^{10} \text{ mL}^{-1}$)
35
36 was compared with an infectivity titer, and indicated that only 0.001% of particles were infectious.
37
38 Elsewhere, Arjmandi *et al.*'s mass measurement technique⁶⁵ was applied to inactivated virions in 75
39
40 mM KCl. Human immunodeficiency virus was measured to be $198 \pm 15 \text{ nm}$ in size with density $1.2 \pm$
41
42 0.1 g cm^{-3} , and Epstein-Barr virions were $170 \pm 13 \text{ nm}$ at a density of $1.7 \pm 0.2 \text{ g cm}^{-3}$. These results
43
44 were comparable with measurements made using rigid etched silicon nanopores and other
45
46
47
48
49 methods.
50

51
52
53 TRPS size and concentration measurements were first applied to bacteria by Roberts *et al.*,⁴ who
54
55 studied the marine cyanobacterium *Prochlorococcus*, and *Baculovirus* occlusion bodies. TRPS size
56
57 distributions for *Prochlorococcus* (range 300-1200 nm with a mean of $\sim 650 \text{ nm}$) and *Baculovirus* (~ 1
58
59
60

1
2
3 μm) agreed with previous reported values. Bacterial concentrations ($6.0 \times 10^8 \text{ mL}^{-1}$ and $9.9 \times 10^7 \text{ mL}^{-1}$
4
5 respectively) were consistent for different users on different days, and lower (by 6% and 17%
6
7 respectively) than measurements using a FC haemocytometer and phase contrast microscopy.
8
9 Accurate determination of *Baculovirus* concentration is vital for insecticide applications. Allen *et al.*⁶⁰
10
11 measured cell size and concentration simultaneously for strains of *Bacillus subtilis* and *Escherichia*
12
13 *coli* during colony growth. TRPS concentrations correlated more closely with colony plating than
14
15 optical density (OD) measurements. Particle volumes between 1.5-10 fL were obtained for each
16
17 sample, consistent with previous work and microscopy, and the cultures incubated with more
18
19 glucose present produced slightly larger values. Bennett *et al.*¹³⁶ found that the bacteria in probiotics
20
21 used in four dairy feed products had similar sizes, in the range 800-2000 nm, with concentrations
22
23 between 4.4×10^9 - $1.2 \times 10^{10} \text{ mL}^{-1}$. In studies of water-borne pathogens which can be harmful to
24
25 humans, Chung *et al.*⁷⁶ compared a wild type strain of *Francisella tularensis* with a mutant, while
26
27 Pang *et al.*¹³⁷ investigated potential surrogates for *Cryptosporidium parvum*. In the former study, the
28
29 mutants ($\sim 750 \text{ nm}$) were slightly larger than wild type bacteria, with longer pulse durations
30
31 suggesting that they also have less negative charge. In the latter, TRPS confirmed that the size of
32
33 protein-modified PS microspheres ($\sim 4.9 \mu\text{m}$, and concentration $2 \times 10^6 \text{ mL}^{-1}$) was similar to *C. parvum*
34
35 oocysts (reproductive cysts containing a zygote).
36
37
38
39
40
41

42 **Other**

43
44 Food and beverage emulsions can be structurally similar to particles such as EVs and liposomes,
45
46 consisting of small capsules stabilized by surfactant molecules. TRPS has been used to characterise
47
48 soy bean oil droplets stabilised by β -lactoglobulin,⁴¹ an emulsion model for milk. The emulsion was
49
50 refrigerated and monitored over four months, during which the modal droplet size increased from
51
52 150 nm to more than 200 nm. The size distribution dynamics inconclusively suggested that the
53
54 dominant growth mechanism involved migration of oil molecules, as in Ostwald ripening, whereas
55
56 aggregation induced by addition of salt was more consistent with flocculation and coalescence. The
57
58
59
60

1
2
3 surface charge of the emulsion droplets was also measured using the variable pressure method.⁷
4
5 Average zeta potentials were calculated using both resistive pulse rate (-18.9 mV) and duration (-
6
7 21.8 mV) data, and were compared with a DLS measurement (-27.6 mV). Beyond emulsions, Gazzola
8
9 *et al.* studied protein haze,¹⁰² a wine quality defect. Aggregation of five wine proteins was analysed
10
11 following different treatments containing phenolics and/or polysaccharide, by measuring aggregate
12
13 sizes from approximately 200 nm to 4000 nm, and concentrations from 2.0×10^5 to 7.5×10^6 mL⁻¹.
14
15

16
17
18 Superparamagnetic beads (SPBs) are widely used in biotechnology, because a magnetic field can
19
20 transport SPBs independently of other interactions.¹³⁸ This is useful for separation, concentration
21
22 and aggregation, and as discussed above SPBs have been used to assist drug delivery,¹³² separation
23
24 in DNA assays,^{72, 103} and efficient separation and aggregation in other targeted assays.^{67, 68} Two
25
26 studies have focussed exclusively on understanding magnetic particle transport in TRPS.^{48, 55} In the
27
28 first, 1 μ m SPBs were used to show how TRPS can be used to detect aggregation.⁴⁸ Upon application
29
30 of a magnetic field, frequently observed larger pulses could be modelled to determine aggregate size
31
32 (Figure 2(b)). An observation of many pulses in close succession suggested that columnar aggregates
33
34 (aligned by their dipole moments) were hydrodynamically separated as they moved through the
35
36 pore. In a more quantitative study of 1.1 μ m SPBs,⁵⁵ a bar magnet generated a magnetic field of up
37
38 to 15 mT at the tunable pore. Beads in the nearer half of the fluid cell were attracted away from the
39
40 pore, reducing the pulse rate and increasing the FWHM duration as the magnet was moved closer.
41
42 Size measurements suggested a lack of aggregation, and it was noted that the particles were at
43
44 relatively low concentration, that aggregates could be sterically excluded from the pore, and that
45
46 hydrodynamic forces in the pore constriction were strong enough to overcome dipole interactions.
47
48
49

50
51
52 Buchs *et al.*¹³⁹ measured the size of selenium (Se) nanoparticles formed by conversion of dissolved
53
54 Se into insoluble, high purity Se by aquatic organisms. The size distribution for these biogenic
55
56 nanoparticles (~360 nm) suggests a mean settling velocity of 2.93 cm per day. Such information
57
58
59
60

1
2
3 could aid the efficient removal of Se nanoparticles from suspension, with positive environmental
4 effects and potential benefits due to demand for Se in dietary supplements and industry, particularly
5 photovoltaics. Yoon *et al.*¹⁴⁰ used TRPS to investigate novel amphiphilic Janus particles synthesized
6 using electrohydrodynamic cojetting, with proposed applications related to self-assembly at
7 interfaces. One population was found to have an average diameter of 2 μm , while the concentration
8 of a second population (average diameter 300 nm determined by DLS) was found to be $5 \times 10^7 \text{ mL}^{-1}$.
9 TRPS has been used to characterize cylindrical micelles which self-assemble from elastin-like
10 polypeptides by genetically fusing an assembly domain to one end. The equivalent diameter (100-
11 150 nm) was broadly in agreement with DLS.⁶⁶ Elsewhere,¹⁴¹ TRPS was an efficient high-throughput
12 method for analysing raspberry-like particles consisting of 4.5 μm PS particles covered by various,
13 smaller microgel spheres in 10 mM formate buffer at pH 3.3.
14
15
16
17
18
19
20
21
22
23
24
25
26
27
28

29 Conclusion

30 Application of TRPS can be summarized by considering the functions served by TRPS in published
31 studies. For particles in complex raw (*e.g.* bodily) fluids, especially EVs, the challenge is to provide
32 useful information while accounting for particles of unknown classification or origin. Key issues for
33 such research include clear specification of the research question, standardized solution
34 preparation, and dealing with highly disperse populations by using multiple pores and considering
35 measurement thresholds. For more controlled environments associated with drug delivery agents
36 and food emulsions (for example), TRPS is usually useful for quality control and could be extended to
37 regulatory compliance. Development of high-quality traceable measurement standards is a
38 challenge for colloidal characterization techniques, and continued comparisons will be of benefit,
39 particularly between physically distinct techniques and particle types. Another broad function of
40 TRPS is monitoring of on-bead chemistry, which is less closely linked to measurement protocols.
41 Development in this area is likely to focus on best practice methods for specific samples and assay
42 targets, with possible diagnostic applications.
43
44
45
46
47
48
49
50
51
52
53
54
55
56
57
58
59
60

1
2
3
4
5 Among many opportunities for new TRPS developments, perhaps the most exciting involve the use
6
7 of actuation to directly interact with particles - trapping, gating^{1,44} or squeezing.⁷⁹ So far, actuation
8
9 has been of most practical benefit for flexible, efficient experimentation, but the effects of
10
11 stretching on measurement have begun to be quantified.^{47,63,125,142} Other opportunities include
12
13 exploration of the fundamental link between electrophoretic mobility measurements and the
14
15 corresponding colloidal surface chemistry. Extraction of particle shape and orientation information
16
17 from TRPS would be of broad interest. Co-ordination of TRPS with optical and plasmonic
18
19 technologies seems likely, as does the eventual application of the technology at molecular length
20
21 scales.
22
23
24
25
26

27 **Acknowledgements**

28
29 This work was supported by a Royal Society of New Zealand Rutherford Discovery Fellowship.
30
31
32
33

34 **References**

- 35
36
37 1 S. J. Sowerby, M. F. Broom and G. B. Petersen, *Sens. Actuators, B*, 2007, **123**, 325.
38
39 2 G. R. Willmott, R. Vogel, S. S. C. Yu, L. G. Groenewegen, G. S. Roberts, D. Kozak, W. Anderson and
40
41 M. Trau, *J. Phys.: Condens. Matt.*, 2010, **22**, 454116.
42
43 3 R. Vogel, G. Willmott, D. Kozak, G. S. Roberts, W. Anderson, L. Groenewegen, B. Glossop, A.
44
45 Barnett, A. Turner and M. Trau, *Anal. Chem.*, 2011, **83**, 3499.
46
47 4 G. S. Roberts, S. Yu, Q. Zeng, L. C. L. Chan, W. Anderson, A. H. Colby, M. W. Grinstaff, S. Reid and R.
48
49 Vogel, *Biosens. Bioelectron.*, 2012, **31**, 17.
50
51 5 G. R. Willmott, S. S. C. Yu and R. Vogel, Proceedings of the 2010 International Conference on
52
53 Nanoscience and Nanotechnology (ICONN), Sydney, 2010.
54
55 6 D. Kozak, W. Anderson, R. Vogel, S. Chen, F. Antaw and M. Trau, *ACS Nano*, 2012, **6**, 6990.
56
57
58
59
60

- 1
2
3 7 R. Vogel, W. Anderson, J. Eldridge, B. Glossop and G. Willmott, *Anal. Chem.*, 2012, **84**, 3125.
4
5 8 E. Weatherall, G. R. Willmott and B. Glossop, Proceedings of the 7th International Conference on
6
7 Sensing Technology (ICST), Wellington, 2013.
8
9 9 D. Kozak, W. Anderson, R. Vogel and M. Trau, *Nano Today*, 2011, **6**, 531.
10
11 10 J. Eldridge, A. Colby, G. R. Willmott, S. Yu and M. Grinstaff, in *Selected Topics in Nanomedicine*, ed.
12
13 T. M. S. Chang, World Science, Singapore, 2013, vol. 3, ch. 10, pp. 219-255.
14
15 11 G. R. Willmott, M. F. Broom, M. L. Jansen, R. M. Young and W. M. Arnold, in *Molecular- and Nano-*
16
17 *Tubes*, ed. O. Hayden and K. Nielsch, Springer New York, 2011, ch. 7, pp. 209-261.
18
19 12 G. R. Willmott and P. W. Moore, *Nanotechnology*, 2008, **19**, 475504.
20
21 13 G. R. Willmott, R. Chaturvedi, S. J. W. Cummins and L. G. Groenewegen, *Exp. Mech.*, 2014, **54**,
22
23 153.
24
25 14 *U. S. Pat.*, 2 656 508, 1953.
26
27 15 R. W. DeBlois and C. P. Bean, *Rev. Sci. Instrum.*, 1970, **41**, 909; R. W. DeBlois, C. P. Bean and R. K.
28
29 A. Wesley, *J. Colloid Interface Sci.*, 1977, **61**, 323.
30
31 16 R. W. DeBlois, E. E. Uzgiris, D. H. Cluxton and H. M. Mazzone, *Anal. Biochem.*, 1978, **90**, 273; R. W.
32
33 DeBlois and R. K. Wesley, *J. Virol.*, 1977, **23**, 227.
34
35 17 B. M. Venkatesan and R. Bashir, *Nat. Nanotechnol.*, 2011, **6**, 615; D. Branton, D. W. Deamer, A.
36
37 Marziali, H. Bayley, S. A. Benner, T. Butler, M. D. Ventra, S. Garaj, A. Hibbs, X. Huang, S. B.
38
39 Jovanovich, P. S. Krstic, S. Lindsay, X. S. Ling, C. H. Mastrangelo, A. Meller, J. S. Oliver, Y. V. Pershin, J.
40
41 M. Ramsey, R. Riehn, G. V. Soni, V. Tabard-Cossa, M. Wanunu, M. Wiggin and J. A. Schloss, *Nat.*
42
43 *Biotechnol.*, 2008, **26**, 1146; D. W. Deamer and D. Branton, *Acc. Chem. Res.*, 2002, **35**, 817; D.
44
45 Deamer, *Annu. Rev. Biophys.*, 2010, **39**, 79.
46
47 18 C. Dekker, *Nat. Nanotechnol.*, 2007, **2**, 209.
48
49 19 M. Rhee and M. A. Burns, *Trends Biotechnol.*, 2007, **25**, 174; K. Healy, B. Schiedt and I. P.
50
51 Morrison, *Nanomedicine*, 2007, **2**, 875; K. Healy, *Nanomedicine*, 2007, **2**, 459; J. J. Kasianowicz, J. W.
52
53 F. Robertson, E. R. Chan, J. E. Reiner and V. M. Stanford, *Annu. Rev. Anal. Chem.*, 2008, **1**, 737; L.-Q.
54
55
56
57
58
59
60

- 1
2
3 Gu and J. W. Shim, *Analyst*, 2010, **135**, 441; F. Haque, J. Li, H.-C. Wu, X.-J. Liang and P. Guo, *Nano*
4
5 *Today*, 2013, **8**, 56; S. Howorka and Z. Siwy, *Chem. Soc. Rev.*, 2009, **38**, 2360; A. Kocera, L. Tauk and
6
7 P. Déjardin, *Biosens. Bioelectron.*, 2012, **38**, 1.
8
9
10 20 L. T. Sexton, L. P. Horne and C. R. Martin, *Mol. BioSyst.*, 2007, **3**, 667.
11
12 21 S. Heider and C. Metzner, *Virology*, 2014, **462-463**, 199.
13
14 22 N. Arjmandi, W. Van Roy, L. Lagae and G. Borghs, *Anal. Chem.*, 2012, **84**, 8490.
15
16 23 S. Park, J. Lim, Y. E. Pak, S. Moon and Y. Song, *Sens. Actuators, B*, 2013, **13**, 6900.
17
18 24 T. Ito, L. Sun and R. M. Crooks, *Anal. Chem.*, 2003, **75**, 2399.
19
20 25 T. Ito, L. Sun, M. A. Bevan and R. M. Crooks, *Langmuir*, 2004, **20**, 6940; T. Ito, L. Sun, R. R.
21
22 Henriquez and R. M. Crooks, *Acc. Chem. Res.*, 2004, **37**, 937.
23
24 26 O. A. Saleh and L. L. Sohn, *Proc. Natl. Acad. Sci. U. S. A.*, 2003, **100**, 820; O. A. Saleh and L. L. Sohn,
25
26 *Nano Lett.*, 2003, **3**, 37.
27
28 27 E. A. Heins, Z. S. Siwy, L. A. Baker and C. R. Martin, *Nano Lett.*, 2005, **5**, 1824.
29
30 28 J. E. Wharton, P. Jin, L. T. Sexton, L. P. Horne, S. A. Sherrill, W. K. Mino and C. R. Martin, *Small*,
31
32 2007, **3**, 1424.
33
34 29 J. D. Uram, K. Ke and M. Mayer, *ACS Nano*, 2008, **2**, 857.
35
36 30 R. An, J. D. Uram, E. C. Yusko, K. Ke, M. Mayer and A. J. Hunt, *Opt. Lett.*, 2008, **33**, 1153.
37
38 31 J. D. Uram, K. Ke, A. J. Hunt and M. Mayer, *Small*, 2006, **2**, 967; J. D. Uram, K. Ke, A. J. Hunt and M.
39
40 Mayer, *Angew. Chem.*, 2006, **118**, 2339.
41
42 32 G. Stober, L. J. Steinbock and U. F. Keyser, *J. Appl. Phys.*, 2009, **105**, 084702.
43
44 33 L. J. Steinbock, G. Stober and U. F. Keyser, *Biosens. Bioelectron.*, 2009, **24**, 2423; S. Umehara, M.
45
46 Karhanek, R. W. Davis and N. Pourmand, *Proc. Natl. Acad. Sci. U. S. A.*, 2009, **106**, 4611.
47
48 34 S. R. German, L. Luo, H. S. White and T. L. Mega, *J. Phys. Chem. C*, 2013, **117**, 703; W.-J. Lan and H.
49
50 S. White, *ACS Nano*, 2012, **6**, 1757.
51
52 35 G. Wang, B. Zhang, J. R. Wayment, J. M. Harris and H. S. White, *J. Am. Chem. Soc.*, 2006, **128**,
53
54 7679.
55
56
57
58
59
60

- 1
2
3 36 W.-J. Lan, D. A. Holden, J. Liu and H. S. White, *J. Phys. Chem. C*, 2011, **115**, 18445.
4
5 37 R. R. Henriquez, T. Ito, L. Sun and R. M. Crooks, *Analyst*, 2004, **129**, 478.
6
7 38 L. Luo, S. R. German, W.-J. Lan, D. A. Holden, T. L. Mega and H. S. White, *Annu. Rev. Anal. Chem.*,
8
9 2014, **7**, 16.1.
10
11 39 S. Wu, S. R. Park and X. S. Ling, *Nano Lett.*, 2006, **6**, 2571.
12
13 40 W.-J. Lan, D. A. Holden, B. Zhang and H. S. White, *Anal. Chem.*, 2011, **83**, 3840.
14
15 41 J. A. Somerville, G. R. Willmott, J. Eldridge, M. Griffiths and K. M. McGrath, *J. Colloid Interface Sci.*,
16
17 2013, **394**, 243.
18
19 42 J. A. Eldridge, G. R. Willmott, W. Anderson and R. Vogel, *J. Colloid Interface Sci.*, 2014, **429**, 45.
20
21 43 G. R. Willmott and B. E. T. Parry, *J. Appl. Phys.*, 2011, **109**, 094307.
22
23 44 G. S. Roberts, D. Kozak, W. Anderson, F. M. Broom, R. Vogel and M. Trau, *Small*, 2010, **6**, 2653.
24
25 45 G. Willmott and R. Young, *AIP Conf. Proc.*, 2009, **1151**, 153.
26
27 46 M. L. Jansen, G. R. Willmott, I. Hoek and W. M. Arnold, *Measurement*, 2013, **46**, 3560.
28
29 47 D. Kozak, W. Anderson, M. Grevett and M. Trau, *J. Phys. Chem. C*, 2012, **116**, 8554.
30
31 48 G. R. Willmott, M. Platt and G. U. Lee, *Biomicrofluidics*, 2012, **6**, 014103.
32
33 49 P. Hauer, E. C. L. Ru and G. R. Willmott, *J. Appl. Phys.*, submitted.
34
35 50 W. Lan, C. Kubeil, J. Xiong, A. Bund and H. S. White, *J. Phys. Chem. C*, 2014, **118**, 2726.
36
37 51 G. R. Willmott and B. G. Smith, *ANZIAM J.*, 2014, **55**, 197.
38
39 52 E. C. Gregg and K. D. Steidley, *Biophys. J.*, 1965, **5**, 393.
40
41 53 J. E. Hall, *J. Gen. Physiol.*, 1975, **66**, 531.
42
43 54 R. B. Schoch, J. Han and P. Renaud, *Rev. Mod. Phys.*, 2008, **80**, 839.
44
45 55 G. R. Willmott, M. G. Fisk and J. Eldridge, *Biomicrofluidics*, 2013, **7**, 064106.
46
47 56 P. Terejanszky, I. Makra, P. Furjes and R. E. Gyurcsanyi, *Anal. Chem.*, 2014, **86**, 4688.
48
49 57 L. Bacri, A. G. Oukhaled, B. Schiedt, G. Patriarache, E. Bourhis, J. Gierak, J. Pelta and L. Auvray, *J.*
50
51 *Phys. Chem. B*, 2011, **115**, 2890.
52
53 58 G. R. Willmott and B. G. Smith, *Nanotechnology*, 2012, **23**, 088001.
54
55
56
57
58
59
60

- 1
2
3 59 S. Lee, Y. Zhang, H. S. White, C. C. Harrell and C. R. Martin, *Anal. Chem.*, 2004, **76**, 6108.
4
5 60 C. S. Allen, J. F. C. Loo, S. Yu, S. K. Kong and T.-F. Chan, *Appl. Microbiol. Biotechnol.*, 2014, **98**, 855.
6
7 61 L. Yang, M. F. Broom and I. G. Tucker, *Pharm. Res.*, 2012, **29**, 2578.
8
9 62 J. de Vrij, S. L. N. Maas, M. van Nispen, M. Sena-Esteves, R. W. A. Limpens, A. J. Koster, S.
10
11 Leenstra, M. L. Lamfers and M. L. D. Broekman, *Nanomedicine*, 2013, **8**, 1443.
12
13 63 E. van der Pol, F. A. W. Coumans, A. E. Grootemaat, C. Gardiner, I. L. Sargent, P. Harrison, A. Sturk,
14
15 T. G. van Leeuwen and R. Nieuwland, *J. Thromb. Haemostasis*, 2014, **12**, 1.
16
17 64 W. Anderson, D. Kozak, V. A. Coleman, Å. K. Jämting and M. Trau, *J. Colloid Interface Sci.*, 2013,
18
19 **405**, 322.
20
21 65 N. Arjmandi, W. V. Roy and L. Lagae, *Anal. Chem.*, 2014, **86**, 4637.
22
23 66 J. R. McDaniel, I. Weitzhandler, S. Prevost, K. B. Vargo, M.-S. Appavou, D. A. Hammer, M.
24
25 Gradzielski and A. Chilkoti, *Nano Lett.*, 2014, **14**, 6590.
26
27 67 M. Platt, G. R. Willmott and G. U. Lee, *Small*, 2012, **8**, 2436.
28
29 68 E. R. Billinge, J. Muzard and M. Platt, *Nanomaterials and Nanosciences*, 2013, **1**, 1.
30
31 69 Y. S. Ang and L.-Y. L. Yung, *ACS Nano*, 2012, **6**, 8815.
32
33 70 D. Kozak, M. Broom and R. Vogel, *Curr. Drug Delivery*, 2014, DOI:
34
35 10.2174/1567201811666140922110647
36
37 71 S. L. N. Maas, J. de Vrij, E. J. van der Vlist, B. Geragousian, L. van Bloois, E. Mastrobattista, R.
38
39 Schiffelers, M. H. M. Wauben, M. L. Broekman and E. N. M. Nolte, *J. Controlled Release*, 2014, **200**,
40
41 87.
42
43 72 M. Adela Booth, R. Vogel, J. M. Curran, S. Harbison and J. Travas-Sejdic, *Biosens. Bioelectron.*,
44
45 2013, **45**, 136.
46
47 73 M. Low, S. Yu, M. Y. Han and X. Su, *Aust. J. Chem.*, 2011, **64**, 1229.
48
49 74 O. A. Alsager, S. Kumar, G. R. Willmott, K. P. McNatty and J. M. Hodgkiss, *Biosens. Bioelectron.*,
50
51 2014, **57**, 262.
52
53
54
55
56
57
58
59
60

- 1
2
3 75 Y.-T. Chiang, Y.-T. Cheng, C.-Y. Lu, Y.-W. Yen, L.-Y. Yu, K.-S. Yu, S.-Y. Lyu, C.-Y. Yang and C.-L. Lo,
4
5 *Chem. Mater.*, 2013, **25**, 4364.
6
7 76 M.-C. Chung, S. Dean, E. S. Marakasova, A. O. Nwabueze and M. L. v. Hoek, *PLoS One*, 2014, **9**,
8
9 e93119.
10
11 77 J.-M. Rabanel, P. Hildgen and X. Banquy, *J. Controlled Release*, 2014, **185**, 71.
12
13 78 Z. Varga, Y. Yuana, A. E. Grootemaat, E. van der Pol, C. Gollwitzer, M. Krumrey and R. Nieuwland,
14
15 *J. Extracell. Vesicles*, 2014, **3**, 23298.
16
17 79 A. Colby, Y. Colson and M. W. Grinstaff, *Nanoscale*, 2013, **5**, 3496.
18
19 80 C. Lee, C. Cottin-Bizonne, A.-L. Biance, P. Joseph, L. Bocquet and C. Ybert, *Phys. Rev. Lett.*, 2014,
20
21 **112**, 244501.
22
23 81 M. Belkin, S.-H. Chao, G. Giannetti and A. Aksimentiev, *J. Comput. Electron.*, 2014, **13**, 826.
24
25 82 J. Menestrina, C. Yang, M. Schiel, I. V. Vlassiouk and Z. S. Siwy, *J. Phys. Chem. C*, 2014, **118**, 2391.
26
27 83 E. Weatherall and G. R. Willmott, submitted,
28
29 84 C. Heitzinger and C. Ringhofer, *J. Comput. Electron.*, 2014, **13**, 801.
30
31 85 S. K. Brar, *Trends in Analytical Chemistry*, 2011, **30**, 4.
32
33 86 N. C. Bell, C. Minelli, J. Tompkins, M. M. Stevens and A. G. Shard, *Langmuir*, 2012, **28**, 10860.
34
35 87 E. van der Pol, A. G. Hoekstra, A. Sturk, C. Otto, T. G. van Leeuwen and R. Nieuwland, *J. Thromb.*
36
37 *Haemostasis*, 2010, **8**, 2596.
38
39 88 R. F. Domingos, M. A. Baalousha, Y. Ju-Nam, M. M. Reid, N. Tufenkji, J. Lead, G. G. Leppard and K.
40
41 J. Wilkinson, *Environ. Sci. Technol.*, 2009, **43**, 7277.
42
43 89 M. Salih, R. Zietse and E. J. Hoorn, *Am J Physiol Renal Physiol*, 2014, **306**, F1251.
44
45 90 N. Kathe, B. Henriksen and H. Chauhan, *Drug Dev. Ind. Pharm.*, 2014, **40**, 1565.
46
47 91 A. K. Pal, I. Aalaei, S. Gadde, P. Gaines, D. Schmidt, P. Demokritou and D. Bello, *ACS Nano*, 2014, **8**,
48
49 9003.
50
51 92 A. N. Böing, J. Stap, C. M. Hau, G. B. Afink, C. Ris-Stalpers, E. A. Reits, A. Sturk, C. J. F. van Noorden
52
53 and R. Nieuwland, *Biochim. Biophys. Acta, Mol. Cell Res.*, 2013, **1833**, 1844.
54
55
56
57
58
59
60

- 1
2
3 93 T. Burnouf, H. A. Goubran, M.-L. Chou, D. Devos and M. Radosevic, *Blood Rev.*, 2014, **28**, 155.
4
5 94 D. Patko, B. Gyorgy, A. Nemeth, K. E. Szabó-Taylor, A. Kittel, E. I. Buzás and R. Horvath, *Sens.*
6
7 *Actuators, B*, 2013, **188**, 697.
8
9 95 R. E. Lane, D. Korbie, W. Anderson, R. Vaidyanathan and M. Trau, *Sci. Rep.*, 2015, **5**, 7639.
10
11 96 K. Farkas, L. Pang, S. Lin, W. Williamson, R. Easingwood, R. Fredericks, M. Jaffer and A. Varsani,
12
13 *Food Environ. Virol.*, 2013, **5**, 231.
14
15 97 F. A. W. Coumans, E. van der Pol, A. N. Böing, N. Hajji, G. Sturk, T. G. van Leeuwen and R.
16
17 Nieuwland, *J. Extracell. Vesicles*, 2014, **3**,
18
19 98 E. van Bracht, S. Stolle, T. G. Hafmans, O. C. Boerman, E. Oosterwijk, T. H. van Kuppevelt and W. F.
20
21 Daamen, *Eur. J. Pharm. Biopharm.*, 2014, **87**, 80.
22
23 99 A. K. L. Yang, H. Lu, S. Y. Wu, H. C. Kwok, H. P. Ho, S. Yu, A. K. L. Cheung and S. K. Kong, *Anal. Chim.*
24
25 *Acta*, 2013, **782**, 46.
26
27 100 A. K. L. Cheung, A. K. L. Yang, B. H. Ngai, S. C. Samuel, M. Gao, P. M. Lau and S. K. Kong, *Analyst*,
28
29 2015, DOI: 10.1039/c4an02079k.
30
31 101 J. Parmentier, N. Thomas, A. Müllertz, G. Fricker and T. Rades, *Int. J. Pharm.*, 2012, **437**, 253.
32
33 102 D. Gazzola, S. C. Van Sluyter, A. Curioni, E. J. Waters and M. Marangon, *J. Agric. Food Chem.*,
34
35 2012, **60**, 10666.
36
37 103 M. Kühnemund and M. Nilsson, *Biosens. Bioelectron.*, in press.
38
39 104 E. R. Billinge, M. Broom and M. Platt, *Anal. Chem.*, 2014, **86**, 1030.
40
41 105 K. K. Lai, R. Renneberg and W. C. Mak, *RSC Adv.*, 2014, **4**, 11802.
42
43 106 B.-T. Pan and R. M. Johnstone, *Cell*, 1983, **33**, 967; C. Harding, J. Heuser and P. Stahl, *Eur. J. Cell*
44
45 *Biol.*, 1984, **35**, 256; G. Raposo, H. W. Nijman, W. Stoorvogel, R. Liejendekker, C. V. Harding, C. J.
46
47 Melief and H. J. Geuze, *J. Exp. Med.*, 1996, **183**, 1161.
48
49 107 S. El Andaloussi, I. Mäger, X. O. Breakefield and M. J. A. Wood, *Nat. Rev. Drug Discovery*, 2013,
50
51 **12**, 347.
52
53 108 We treat the terms microRNA (miRNA) and messenger RNA (mRNA) as synonyms.
54
55
56
57
58
59
60

- 1
2
3 109 G. Raposo and W. Stoorvogel, *J. Cell Biol.*, 2013, **200**, 373.
4
5 110 R. van der Meel, M. Krawczyk-Durka, W. W. van Solinge and R. M. Schiffelers, *International*
6
7 *Journal of Laboratory Hematology*, 2014, **36**, 244.
8
9 111 F. Momen-Heravi, L. Balaj, S. Alian, J. Tigges, V. Toxavidis, M. Ericsson, R. J. Distel, A. R. Ivanov, J.
10
11 Skog and W. P. Kuo, *Front. Physiol.*, 2012, **3**, 354; E. van der Pol, F. Coumans, Z. Varga, M. Krumrey
12
13 and R. Nieuwland, *J. Thromb. Haemostasis*, 2013, **11**, 36; K. W. Witwer, E. I. Buzás, L. T. Bemis, A.
14
15 Bora, C. Lässer, J. Lötvall, M. G. Piper, S. Sivaraman, J. Skog and C. Théry, *J. Extracell. Vesicles*, 2013,
16
17 **2**, 20360; P. Hexley, K. P. Rismiller, C. T. Robinson and G. F. Babcock, *Exosomes Microvesicles*, 2014,
18
19 **2**, 1.
20
21 112 K. Shimbo, S. Miyaki, H. Ishitobi, Y. Kato, T. Kubo, S. Shimose and M. Ochi, *Biochem. Biophys.*
22
23 *Res. Commun.*, 2014, **445**, 381.
24
25 113 Izon Science Website, www.izon.com, (accessed November 2014).
26
27 114 L. Cheng, R. A. Sharples, B. J. Scicluna and A. F. Hill, *J. Extracell. Vesicles*, 2014, **3**, 23743.
28
29 115 L. Cheng, X. Sun, B. J. Scicluna, B. M. Coleman and A. F. Hill, *Kidney Int.*, 2014, **86**, 433.
30
31 116 K. D. Connolly, G. R. Willis, D. B. N. Datta, E. A. Ellins, K. Ladell, D. A. Price, I. A. Guschina, D. A.
32
33 Rees and P. E. James, *J. Lipid Res.*, 2014, **55**, 2064.
34
35 117 G. T. Szabó, B. Tarr, K. Pálóczi, K. Éder, E. Lajkó, Á. Kittel, S. Tóth, B. György, M. Pásztói, A.
36
37 Németh, X. Osteikoetxea, É. Pállinger, A. Falus, K. Szabó-Taylor and E. I. Buzás, *Cell. Mol. Life Sci.*,
38
39 2014, **71**, 4055.
40
41 118 T. Katsuda, R. Tsuchiya, N. Kosaka, Y. Yoshioka, K. Takagaki, K. Oki, F. Takeshita, Y. Sakai, M.
42
43 Kuroda and T. Ochiya, *Sci. Rep.*, 2013, **3**, 1197.
44
45 119 Y. H. Ng, S. Rome, A. Jalabert, A. Forterre, H. Singh, C. L. Hincks and L. A. Salamonsen, *PLoS One*,
46
47 2013, **8**, e58502.
48
49 120 H.-I. Chang and M.-K. Yeh, *Int. J. Nanomed.*, 2012, **7**, 49.
50
51 121 ISEV, Proceedings of the Third International Meeting of the International Society for
52
53 Extracellular Vesicles (ISEV), Rotterdam, 2014.
54
55
56
57
58
59
60

- 1
2
3 122 Creative Commons Attribution-Noncommercial 3.0 Unported License
4
5 (<http://creativecommons.org/licenses/by-nc/3.0/>). The original article entitled "Exosomes provide a
6
7 protective and enriched source of miRNA for biomarker profiling compared to intracellular and cell-
8
9 free blood" can be accessed at <http://dx.doi.org/10.3402/jev.v3.23743>. Change made: the TEM
10
11 image inset was originally part of a separate figure.
12
13 123 T. Lammers, F. Kiessling, W. E. Hennink and G. Storm, *J. Controlled Release*, 2012, **161**, 175; M. E.
14
15 Davis, Z. G. Chen and D. M. Shin, *Nat. Rev. Drug Discovery*, 2008, **7**, 771.
16
17 124 V. P. Torchilin, *Pharm. Res.*, 2007, **24**, 1.
18
19 125 E. Garza-Licudine, D. Deo, S. Yu, A. Uz-Zaman and W. B. Dunbar, Proceedings of the 32nd Annual
20
21 International Conference of the IEEE EMBS, Buenos Aires, 2010.
22
23 126 E. van Bracht, R. Raavé, W. P. R. Verdurmen, R. G. Wismans, P. J. Geutjes, R. E. Brock, E.
24
25 Oosterwijk, T. H. van Kuppevelt and W. F. Daamen, *Int. J. Pharm.*, 2012, **439**, 127.
26
27 127 J. A. M. Montanari, P. L. Bucci and S. d. V. Alonso, *Int. J. Res. Pharm. Chem.*, 2014, **4**, 484.
28
29 128 M. T. Burgess and T. Porter, *Proceedings of Meetings on Acoustics*, 2013, **19**, 075059.
30
31 129 L. E. Ruff, E. A. Mahmoud, J. Sankaranarayanan, J. M. Morachis, C. D. Katayama, M. Corr, S. M.
32
33 Hedrick and A. Almutairi, *Integr. Biol.*, 2013, **5**, 195.
34
35 130 M. Naeem, W. Kim, J. Cao, Y. Jung and J.-W. Yoo, *Colloids Surf., B*, 2014, **123**, 271.
36
37 131 M. Pevarnik, M. Schiel, K. Yoshimatsu, I. V. Vlassiouk, J. S. Kwon, K. J. Shea and Z. S. Siwy, *ACS*
38
39 *Nano*, 2013, **7**, 3720; D. A. Holden, J. J. Watkins and H. S. White, *Langmuir*, 2012, **28**, 7572.
40
41 132 A. Amirfazli, *Nat. Nanotechnol.*, 2007, **2**, 467; L. Douziech-Eyrolles, H. Marchais, K. Hervé, E.
42
43 Munnier, M. Soucé, C. Linassier, P. Dubois and I. Chourpa, *Int. J. Nanomed.*, 2007, **2**, 541.
44
45 133 D. Upadhyay, S. Scalia, R. Vogel, N. Wheate, R. O. Salama, P. M. Young, D. Traini and W.
46
47 Chrzanowski, *Pharm. Res.*, 2012, **29**, 2456.
48
49 134 K. Astafyeva, Ph.D. Thesis, Universite Pierre et Marie Curie - Paris VI, 2014.
50
51 135 D. Rybakova, M. Radjainia, A. Turner, A. Sen, A. K. Mitra and M. R. H. Hurst, *Mol. Microbiol.*,
52
53 2013, **89**, 702.
54
55
56
57
58
59
60

1
2
3 136 G. Bennett, R. Rajan, C. R. Bunt and M. A. Hussain, *N. Z. Vet. J.*, 2012, **61**, 119.
4

5 137 L. Pang, U. Nowostawska, L. Weaver, G. Hoffman, A. Karmacharya, A. Skinner and N. Karki,
6
7 *Environ. Sci. Technol.*, 2012, **46**, 11779.
8

9 138 Q. A. Pankhurst, J. Connolly, S. K. Jones and J. Dobson, *J. Phys. D: Appl. Phys.*, 2003, **36**, R167; M.
10
11 A. M. Gijs, *Microfluid. Nanofluid.*, 2004, **1**, 22.
12

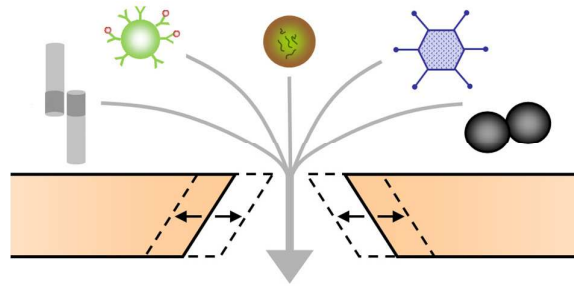
13 139 B. Buchs, M. W. H. Evangelou, L. H. E. Winkel and M. Lenz, *Environ. Sci. Technol.*, 2013, **47**, 2401.
14

15 140 J. Yoon, A. Kota, S. Bhaskar, A. Tuteja and J. Lahann, *ACS Appl. Mater. Interfaces*, 2013, **5**, 11281.
16

17 141 S. Saxena and L. A. Lyon, *J. Colloid Interface Sci.*, 2015, **442**, 39.
18

19 142 D. Kozak, W. Anderson and M. Trau, *Chem. Lett.*, 2012, **41**, 1134.
20
21
22
23
24
25
26
27
28
29
30
31
32
33
34
35
36
37
38
39
40
41
42
43
44
45
46
47
48
49
50
51
52
53
54
55
56
57
58
59
60

Table of contents entry



This Review focusses on the recent surge in applied research using tunable resistive pulse sensing, a technique used to analyse submicron colloids in aqueous solutions on a particle-by-particle basis.

1
2
3
4
5
6
7
8
9
10
11
12
13
14
15
16
17
18
19
20
21
22
23
24
25
26
27
28
29
30
31
32
33
34
35
36
37
38
39
40
41
42
43
44
45
46
47
48
49
50
51
52
53
54
55
56
57
58
59
60

Biographical notes



Eva Weatherall completed an honours degree in chemistry at Victoria University of Wellington in 2011. Following a period of employment at Izon Science, the manufacturer of tunable resistive pulse sensing systems, she commenced PhD studies based at Callaghan Innovation (Lower Hutt, New Zealand) and affiliated to Victoria University in 2013. Her research focuses on protocols for charge measurement using tunable resistive pulse sensing.



Geoff Willmott is a Senior Lecturer in the Departments of Physics and Chemistry at the University of Auckland, New Zealand, and a Principal Investigator with the MacDiarmid Institute for Advanced Materials and Nanotechnology. He started working on tunable resistive pulse sensing more than five years ago, while based at Industrial Research Limited (now Callaghan Innovation, Lower Hutt, New Zealand). His interests range from nanofluidics and soft condensed matter through to dynamic microfluidics and high-speed photography.